NAT'L INST. OF STAND & TECH R.I.C.

A11104 085751

NBSIR 84-2949

Advanced Thin Film Thermocouples

Kenneth G. Kreider*, Stephen Semancik*, and Craig Olson**

*U.S. DEPARTMENT OF COMMERCE
National Bureau of Standards
Center for Chemical Engineering
Chemical Process Metrology Division
Gaithersburg, MD 20899

**U.S. DEPARTMENT OF COMMERCE
National Bureau of Standards
Center for Materials Science
Metallurgy Division
Gaithersburg, MD 20899

October 1984

Contract: C-54715-D

NBSIR 84-2949

ADVANCED THIN FILM THERMOCOUPLES

Kenneth G. Kreider*, Stephen Semancik*, and Craig Olson**

*U.S. DEPARTMENT OF COMMERCE
National Bureau of Standards
Center for Chemical Engineering
Chemical Process Metrology Division
Gaithersburg, MD 20899

**U.S. DEPARTMENT OF COMMERCE
National Bureau of Standards
Center for Materials Science
Metallurgy Division
Gaithersburg, MD 20899

October 1984

Contract: C-54715-D

U.S. DEPARTMENT OF COMMERCE, Malcolm Baldrige, *Secretary*

NATIONAL BUREAU OF STANDARDS, Ernest Ambler, *Director*

FOREWORD

The research performed on this contract is intended to provide information in order to improve the technology of thin film thermocouples for gas turbine engine blades and vanes. Two principal target areas were selected for emphasis. They included the coating-substrate compatibility problem and the properties of the insulating oxide on which the thin film thermocouple is bonded. The insulating oxide must not only provide the electrical insulation for the thermocouple but also must structurally bond the thermocouple to the engine part being measured. Therefore, both insulating and adhesion properties were studied.

The approach included using commercial materials technology up to the fabrication of the insulator and thermocouple followed by mechanical, thermal, and electrical testing of properties. This effort was combined with analytical techniques including optical microscopy, X-ray diffraction, optical interferometry, scanning electron microscopy (SEM), energy dispersive X-ray analysis (EDX), and X-ray photoemission spectroscopy (XPS). We would like to thank James Allen for his help in the fabrication and testing of the test devices. We would like to express appreciation for technical advice to James Mulally and Ralph Hecht of the coatings group at Pratt and Whitney-Florida, William Stowell of the Instrumentation Engineering at General Electric-Cincinnati, and Prof. Fred Pettit of the University of Pittsburgh. We would also like to thank Ray Holanda, the NASA Project Manager for his excellent guidance and technical advice in accomplishing this project.

Table of Contents

Summary

Four substrate-coating combinations were investigated as a materials system base for thin film platinum-platinum 10% rhodium thermocouple sensors. The cobalt-base vane alloy MAR M509 was combined with a sputtered FeCrAlY coating and the nickel-base blade alloy MAR M200+Hf was combined with coating alloys of FeCrAlY and both electron beam and sputter deposited NiCoCrAlY. All combinations were successfully thermally oxidized and sputter coated with Al_2O_3 to form a good insulating foundation for the Pt-Pt10Rh sputter coated thin film thermocouple. Thermal oxidation was performed in air, wet argon, dry argon, and argon with 4% hydrogen to control the rate and morphology of the oxides on the MCrAlY. The best oxides were formed by starting the oxidation in dry argon followed by air atmospheres at 1050-1090°C. Oxides on the NiCoCrAlY were generally smoother and more uniform than those on FeCrAlY. These were characterized using optical micrography, visual inspection, XPS and EDX for composition, and electrical measurements. The thickness, 1.5-2.0 μm, measured by weight gain, was considered optimum.

Aluminum oxide coatings were deposited by reactively sputtering from an aluminum target in Ar+10% O_2 using an RF planar magnetron. These coatings were evaluated microscopically, by interferometry for thickness, by EDX and XPS for composition, for adhesion, and by high temperature electrical testing. XPS studies indicated considerable improvement in composition and insulating properties of the sputtered oxide compared to the thermal oxide. This pure Al_2O_3 should be 1-2 μm thick to avoid shorts and minimize coating stresses that would lead to delamination.

To prevent substrate degradation from interdiffusion with the coating, Al_2O_3 barrier layers were investigated. Sputtered Al_2O_3 in 0.6 and 2.0 μm layers were heat treated and compared with samples containing no barrier

layer using EDX to determine interdiffusion of Al, Fe, Ni, Co, and Cr. It was apparent that bridging of the barrier layer by the FeCrAlY coating nullified the effectiveness of the barrier layer.

The platinum-platinum 10% rhodium thin film thermocouples were sputter deposited to a thickness of approxmately 1.5 μm. These were evaluated for adherence, high temperature stability against shorting and material loss, and for thermocouple e.m.f. Thin films of less than 1 μm tended to last less than 20 hrs at 1050°C. Some problems of platinum film adherence in high temperature cycling were encountered and may need further attention. These problems may be alleviated using an improved treatment or a reactive metal bond enhancer in the system.

I. INTRODUCTION

Conventional surface measurement techniques on turbine airfoils perturb the boundary layer on the surface of an airfoil or the heat flows within the airfoil to the extent that detailed analyses of data are quite difficult. This problem is particularly acute in cooled turbine airfoils, where increases in the turbine inlet temperatures have been accompanied by complex air and water cooling designs and attendant reductions of the component cross section. To meet this need, a new technology for constructing arrays of thin, insulated, sensing films directly on turbine airfoil surfaces must be developed.

While the use of thin film sensors for low temperature surface measurements has been common for some time (1,2,3), practical thin film devices for use in harsh environments must satisfy several design constraints which preclude the use of conventional methods and materials [and severely limit the choice of alternate materials and techniques of construction].

There is a new method of construction of high temperature thin films which has provided the first thin film turbine airfoil devices in large scale aircraft gas turbines (4,5). A brief review of this technology indicates the potential and the problems of high temperature thin film devices in gas turbines. The existing method of high temperature thin film construction uses a thermally grown metal oxide to electrically insulate the sensing element from the substrate (6-9). In this technique, a turbine component is coated with an alloy capable of growing an adherent, high dielectric strength metal oxide. The coated component is then oxidized and arrays of sensors and leads are sputtered on the oxidized surfaces. Wire leads are attached to the sensors and the assembly is reoxidized. The development of practical surface sensors for use in harsh environments is primarily dependent on the development of a coating which is compatible with the substrate material and capable of growing useful insulating

surface oxide layers. For turbine alloys, the nickel base alloy NiCoCrAlY and the iron base alloy, Fe 18Cr 11Al 0.7Y, have been selected from the group of MCrAlY high temperature alloys which form adherent aluminum oxides during oxidation. An extensive investigation of the electrical properties of the aluminum oxides grown on these alloys led to the initial selection of FeCrAlY by Dils (10). The dielectric strengths of oxides grown on this alloy ($>5 \times 10^4$V/ cm at 1093°C) are high and the conductivities of the oxides $10^{-8}\Omega^{-1}$ at 1093°C) are low. In addition, the alloy has desirable mechanical properties throughout the operating range of the sensors and devices using this alloy are unusually durable. Similar properties of the native oxide on NiCoCrAlY and its commercial use in coating materials for turbine engine hardware has led to its selection.

Each element of the sensor is chosen for its specific electrical, chemical, or mechanical properties and, as a result, it is necessary to combine materials with widely varying types of chemical bonding. The metal oxide is an insulator with strong ionic bonds, the coating is a high temperature metal alloy and the sensing element is usually a noble metal alloy. Therefore, when the temperature of the assembly is changed, thermal mechanical strains develop within the assembly. In a gas turbine, the assembly experiences thermal mechanical strains during normal operation. When the engine is decelerated from takeoff to idle, high compressive strains are developed in the uniform oxide layer (11,12). At imperfections in the oxide, shear tractions are applied to the metal/metal oxide interface and cause a concentration of inplane stresses at the interface. In addition, the combustor exhaust gases induce small, high frequency temperature oscillations at the metal surface; in the typical gas turbine, the oxide and metal coating near the surface oscillate $\pm$5°C several times a second(12). These temperature oscillations induce only a $\pm$60 μm/m strain ($\pm$21 MN/m^2 stress)

in the oxide and a +120 μm/m strain ($\pm$ 12 MN/m^2 stress) in the coating but the latter strain is adequate to cause plastic deformation of coatings which are sufficiently weak and ductile to accommodate the strains associated with the large infrequent temperature cycles. The deformation of the substrate displaces the surface material into the boundary layer where the oxide and metal are apparently subjected to additional large heat flows (13).

The resultant thermal mechanical strains within the assembly can be accommodated by a limited number of techniques. A scanning electron microscope study of devices after extensive use in laboratory combustor exhaust gases has indicated that, in general, the thermal strain in useful (< 1-2 μm) thin oxides is stored as elastic strain energy in the oxide, while strain relief in usable thick (2-5 μm) oxides occurs by buckling and attendant plastic deformation of the substrate (11). It has been concluded that, in order for the sensor assembly to remain intact, it is necessary to select a system in which: 1) the compressive shear stress of the oxide is greater than the buckling stress of the oxide when it is attached to the coating, 2) the metal oxide/metal interface yield and shear strengths are greater than the coating yield strength, 3) the coating yield strength is small and 4) the coating is ductile over the entire operating range of the sensors. In successful devices, the coating is sufficiently uniform that the oxide layer remains attached to the coating and continues to insulate the sensing film from the coatings. NiCoCrAlY and FeCrAlY satisfy these requirements; their oxides are adherent and the material is sufficiently ductile throughout the operating range that thermal strain relief occurs primarily by oxide buckling and regeneration by deformation of the MCrAlY.

The thermal mechanical strains across the noble metal/oxide interface are much smaller since the thermal expansion coefficients of both materials are similar and the yield stress of the noble metal is low. However, it was found

3

that high velocity combustor exhaust gas flow over the sensors does cause delamination of the sensing elements deposited on smooth oxide surfaces. There is little chemical bonding between aluminum oxide and useful noble metal alloys and, therefore, the coating is abraded before oxidation in order to cause the growth of an irregular oxide. The films are then sputtered into the irregular surface and interlocked with the oxide.

However, several problems remain in order to achieve a practical technology that can be used in a routine manner in the gas turbine industry (6). This investigation addresses the critical problem identified by the above mentioned reference (7-9). These are areas of immediate concern which have resulted in insufficient film adhesion, metal oxide insulation failures, and degradation of the substrate alloy properties.

Initial studies have indicated that those coatings which form the highest dielectric strength oxide may be unstable on nickel base alloys. Interdiffusion between a coating and an alloy can cause a loss of adhesion of the oxide film, and more importantly, may weaken the thin substrate alloy. It is essential that the sensor technology employ a coating that will not reduce the life of the turbine component. The properties of the oxide layer are also critical. Specifically, the interrelationshps between the dielectric properties of the oxide layer, the adhesion of the oxide to the coating, and the adhesion of the noble metal films to the oxide must be considered. As described above, there are relatively few coatings which accommodate the thermal mechanical strains within the sensor. The properties of the coating also effect the electrical breakdown of the oxide. The morphology of the oxide affects the oxide adhesion, electrical breakdown of the oxide and the adherence of the noble metal thin film. A successful sensor technology will balance the effects of the coating, surface

morphology oxidation cycles and sputtered aluminum oxide films on the oxide properties.

II. EXPERIMENTAL MATERIALS AND METHODS

A. Material Selection and Procurement

The most important planned application for the thin film sensors is in the hot section of the gas turbine engine. Both blades and vanes have significant needs for accurate surface temperature measurements in commerical and military engines. Discussions with General Electric (14) and Pratt and Whitney (14) engineers were used to select the candidate materials. Both GE and P&WA selected MAR M509 as the vane alloy; P&WA selected MAR M200 + Hf as the blade alloy and GE selected Re 80H. Subsequent negotiations to obtain the materials from the manufacturers favored the MAR M200 + Hf and the MAR M509. The standard coating techniques include the pack cementation Co-Dep process, sputtered MCrAlY and electron beam (EB) coating. Since the latter two coating techniques are used on the selected substrate alloys, EB and sputtering were chosen for the coatings. The EB coating of NiCoCrAlY could be commercially prepared and purchased to specification on the MAR M200 + Hf and it was selected as one of the coating-substrate combinations. It was procured from Chromalloy and our samples were designated with a "C". The sputtered coatings could also be procured from Pratt and Whitney: both FeCrAlY and NiCoCrAlY on both the MAR M200 + Hf and MAR M509. This approach has several advantages: it ensures that the material systems represent the state of the art in advanced turbine engine material technology, and it simplifies the transfer of gained technology to commercial practice.

The selection of coating alloys was based on two premises: first, the NiCoCrAlY should be investigated because it was the most successful coating for

5

the MAR M200 + Hf and we could study two deposition techniques and compositions; second FeCrAlY had been proposed by Dils with support from P&WA as a possible improvement on the system with the hope that the oxide dielectric capabilities and adhesion would be superior. In summary, Table 1 is a list of the alloys investigated with their nominal compositions and Table 2 is a list of the combinations investigated with their designations.

For all studies of dielectric strength, adhesion, and thermocouple properties, the above materials were procured from P&WA and Chromalloy without any problems. For the substrate-coating stability tests, an intermediate layer of Al_2O_3 was sputtered between the MCrAlY and substrate alloy. These samples were also procured but considerable problems were encountered in obtaining coatings with adequate adherence to the Al_2O_3. The standard procedure for obtaining good adherence to the substrate is to abrade the surface with 50 μm glass shot peening thus giving the coating more purchase. This technique can lead to "leaders" or imperfections which might shunt the Al_2O_3 diffusion barrier and therefore an optical polish was used to insure a high quality Al_2O_3 coating. Unfortunately, the adherence problem marred the benefits of this approach.

B. Test Coupon Design

The test coupon design for this investigation is intended to simulate the applications of thin film thermocouples on present and near future turbine engine first stage turbine blades and vanes. The materials of construction of that hardware was discussed above in II-A but other considerations are also important in the design of the test coupon. A schematic cross section of the thin film sensor is presented in Figure 1 with the thickness of each layer of the device. These thickness relationships must be preserved in the test coupon

6

design to preserve the thermal expansion relationships and simulate the stress and strain environment of the actual application. Actual first stage blades in engines are typically 4-5 cm long and 0.3 to 1.0 cm in thickness with internal cooling passages. These dimensions are so large compared to the layer thicknesses of the gage that it was felt test coupons 2 cm x 2 cm x 0.5 cm would properly relate the blade and vane dimensions. Essentially, the substrate material MAR M509 or MAR M200 + Hf determines the thermal expansion of the structure in both the engine hardware and test coupon. All the test coupons used in the investigation were prepared and coated by commercial processes to insure direct correspondences of metallurgical structural aspects.

The test coupon design also had the following requirements. It must be suitable for thermal oxidation; surface grinding, polishing, and cleaning; sputtering of uniform layers; electrical performance evaluation up to 1100°C; optical and electron microscopic analysis; analysis by energy dispersive X-ray analysis and X-ray photoemission spectroscopy; and evaluation as a thermocouple. To efficiently and economically satisfy the above requirements, a flat test coupon approximately 2 x 2 x 0.5 cm was employed which was suitable for all but the last requirements. Only the determination of diffusion profiles for the barrier layer investigation of the coating-substrate stability tests required a destructive (sectioning) analysis of the test coupon. The requirement of evaluating thermocouple performance, however, dictates that the legs of the thermocouple pass through the thermal gradient from the connections to the measured temperature at the junction. This thermocouple evaluation requires a long test coupon so that the dimensions of 10 x 0.5 x 0.5 cm were chosen for this test. Both test coupons could be processed in a virtually identical manner throughout the fabrication procedure. A metal masking technique was chosen for obtaining the thermocouple pattern. Steel shimstock 0.12 mm thick was chosen as the masking

7

material and it could be cut accurately to approximately 0.3 mm tolerances. The thermocouple pattern for the test bars included 1.0 mm wide legs spaced 1.0 mm apart. A diamond saw was used to cut the masking slot. Although placement of the masks on the samples was done by hand (no precision fixtures were employed) alignment was adequate for two legged thermocouples on a 0.5 cm wide bar. Estimated resolution of this technique is approximately 0.1 mm but this could be improved with fixtures.

C. Cleaning and Oxidation Procedures

The MCrAlY coating test samples were received with a nodular surface which was ground and polished to prepare the surface for oxidation. Electron beam deposited NiCoCrAlY samples have a "matte" finish and required only 600 grit preparation. These "C" samples were all ground with 600 grit paper and some received a polish with 1 μm diamonds followed by a 50 μm shot peening with glass spheres. Since no advantage was perceived comparing the shot peening to the 600 grit polish, the shot peening was discontinued. Following the 600 grit polish, the cleaning procedure included an alconox detergent followed by water rinse, ultrasonic cleaning in acetone, methyl alcohol rinse and de-ionized water rinse. Samples were handled only with tongs and rubber gloves when clean. The sputtered coatings required more grinding (400 mesh) to obtain a flat, smooth surface and FeCrAlY coatings in some cases required considerable surface removal (10-20 μm). In fact, pits and defects in the FeCrAlY were a problem in surface preparation and caused the rejection of some samples.

The recommended oxidation treatment for the NiCoCrAlY coatings by Grant and Przybyszewski[7] includes 4 hours at 1350K in dry hydrogen followed by 50 hours at 1300K in air. They recommend that pO_2 be kept below 10^{-5} Pa in the early stages of oxidation to suppress the formation of chromium and cobalt

8

oxides during the initial Al_2O_3 formation and to start the migration of aluminum toward the surface. This approach promotes the gradual growth of a dense, hard, and adherent layer of Al_2O_3. Both argon and dry hydrogen have been suggested to achieve this selective oxidation and it was decided to investigate the relative advantages of various partial pressures of oxygen and water vapor. Oxide formation on MCrAlY alloys has been studied in depth and reported in the literature[10,11,15-25]. In addition, the authors consulted with GE and P&WA engineers and Prof. Fred Pettit[15,17] (U. Pittsburgh) to determine the most useful approach in achieving the optimum thermal oxide on the specific FeCrAlY and NiCoCrAlY alloys used in this investigation. The desired properties of the oxide are that it be durable and self healing, have excellent insulating and dielectric properties, and provide for good adhesion of the lamellae of the thin film sensor. Experiments were designed to analyze and test the oxide for its morphology, uniformity, electrical properties, thermal cycling stability, and adhesion. These experiments will be described in subsequent sections.

The elements in the MCrAlY coatings have various rates of oxidation depending on the temperature, partial pressure of oxygen, concentration of the metal species at the reacting surface, and the free energy of formation of the oxide formed. Selective oxidation of one or more species can be most effectively controlled by controlling the partial pressure of oxygen. Thus, by maintaining pO_2 to below 10^{-7} Pa (10^{-12} atm) at 1000°C only the aluminum and yttrium will form oxides. Above this range, chromium oxidizes and above 0.1 Pa (10^{-6} atm) nickel, cobalt and iron oxides form. The method used in this investigation included oxidation with argon plus 4% hydrogen to suppress the formation of chromium oxides ($pO_2 < 10^{-7}$ Pa); and argon with both dry ($pO_2 < 1$ Pa), and wet ($pO_2 = 1$ Pa, $pH_2O = 3000$ Pa) argon to suppress cobalt,

nickel, and iron oxides; and air for the final oxide growth. Once Al_2O_3 is formed, further oxide growth is primarily Al_2O_3 because of the diffusion and kinetics of the oxide formation process. In fact, the MCrAlY alloys were designed to form the Al_2O_3 as a protective barrier for turbine engine hardware. Its stability and extremely low diffusion coefficients make the Al_2O_3 superior for oxidation protection as well as being useful as an electrical insulating layer for the thin film sensors. For use as an insulating layer in a thin film sensor, however, the purity and continuity requirements are most stringent. Therefore, suppression of formation of any oxide such as a nickel oxide which would have inferior electrical properties is important. The detection of iron, nickel, and cobalt oxides is simple since these oxides have characteristic colors and are apparent in visual inspection. Photomicrography at 500X is also useful to detect inclusions, second phase oxides, and other perturbing irregularities in the alumina film which are detrimental to the electrical properties of the films.

The thermal oxidation was performed using the four different atmospheres described above at temperatures between 975 and 1120°C for periods up to 80 hours on both the FeCrAlY and NiCoCrAlY alloys. Thickness and quality of the oxide was monitored by recording weight gain and microscopic evaluation.

D. Sputter Coating

The FeCrAlY and NiCoCrAlY sputtered coatings were procured from Pratt and Whitney Aircraft. NiCoCrAlY coatings were approximately 0.1 mm thick and had an as deposited composition of 0.573 Ni, 0.152 Co, 0.167 Cr, 0.108 Al, and 0.0013Y weight fractions as determined from electron microprobe measurements. A photomicrograph of the coating after heat treatment of 1075°C for 4 hours in argon is given in Fig. 2. The two phase structure of the $\gamma - \gamma'$ is apparent. Fig. 3

is a yttrium X-ray map indicating that the yttrium was not lost and still has broad distribution in the coating thereby implying that its use in improving bonding is preserved through the sputtering operation. The FeCrAlY coatings were measured to have a composition of Fe plus 0.17 Cr, 0.11 Al, 0.003 Si, and 0.001Y (weight fractions). A 1000X photomicrograph is shown in Fig. 4 which indicates the faceted growth and the need for significant material removal to obtain a smooth surface.

In-house sputtering included the reactive sputtering of Al_2O_3 and RF magnetron sputtering of platinum and platinum 10%-rhodium thermocouple alloys. The sputtering was accomplished using a Varian (14) 3118 vacuum sputtering chamber and Plasmatherm (14) HFS-3000D RF generator (3000 watt) at 13.56 MHz, Plasmatherm (14) 3000 AMSE impedance matching box, and a 5 cm magnetron of the type sold by U.S. Guns (14). An Inficon (14) IC 6000 quartz oscillator thickness gauge was used to monitor the deposition during sputtering and a mass spectrometer was used for residual gas analysis. Bottled UPC 99.999% Argon and HP 99.99% oxygen were used as the sputtering gases. Typical parameters for platinum and platinum + 10% rhodium sputtering were: target to substrate distance 15-25 cm; initial vacuum $4-15 \times 10^{-5}$ Pa; argon sputtering pressure 0.14 Pa; 250 watts power; deposition rates 0.4-0.8 nm per sec metal; and RF impedance 50 ohms. The reflected power was less than 1%. Typical parameters for reactive sputtering of Al_2O_3 were: aluminum target, target to substrate distance, 15 cm, initial vacuum 4×10^{-5} to 1.4×10^{-4} Pa; argon pressure 0.14 Pa oxygen pressure 0.014 Pa, 300 watts power, deposition rates 0.05-0.1 nm per second, and RF impedance 50 ohms. Typical residual gas analysis from the mass spectrometer indicated the following pressures: $H_2O=10^{-4}$, Ar= 10^{-6}, $O_2=10^{-5}$, CO-$N_2=3 \times 10^{-5}$, $CH_4=5 \times 10^{-6}$ Pa. The thickness of deposition was checked by weight gain on the sample and monitored on a glass slide. The glass

11

slide is also a convenient way to insure the stoichiometry of the Al_2O_3 since any problems affect the transparency of the deposit. Thickness of the Al_2O_3 deposits was also checked using interferometers with thallium illumination which indicated fringes at step heights of 0.27 μm.

E. Thermal, Mechanical, and Electrical Testing

Several thermal, mechanical and electrical tests were used to evaluate the adhesion, stability, electrical performance, and overall suitability of the aluminum oxide coatings and platinum-platinum rhodium thermocouple films. They included a mechanical adhesion test, electrical insulation and dielectric performance at temperature test, a thermal cycling stability test, and a thermocouple performance test. The adhesion test employed a commercial Sebastian (14) adhesion tester which operates by pulling an epoxy bonded tab from the bonded film. These tests are reported directly as a shear strength of the fiber bond or strength up to 10,000 psi.

The electrical insulation and dielectric test is performed using the test jig pictured in Fig. 5. The 2 cm x 2 cm test coupon is held with platinum and platinum-10% rhodium connections to the thin film thermocouple electrodes described in Section IIB and heated to 1075°C in an air furnace. The output voltage and resistance with a one volt potential are monitored between the Pt and PtRh thin film and between the thin film and substrate (ground) while heating the test coupon. This test detects any premature dielectric breakdown of the insulator and any instability of the thin film sensor. Although the test cannot insure the stability of the thermocouple emf since the entire thin film thermocouple is at virtually one temperature, it does detect increases in resistance or deterioration mechanisms such as oxidation of rhodium during high temperature exposure.

12

The thermal cycling test is also performed on the 2 cm square test coupon by cycling the coupon to 1000°C. The heating cycle is generated by a propane air torch in 60-90 seconds and cooling to below 100°C is also accomplished in less than 120 seconds. Temperatures were measured with a carefully placed thermocouple and by optical pyrometry. Both techniques for measurement underestimate the maximum temperature of the thin film itself which tends to develop hot spots as defects are generated. This test detects adhesion problems as well as overall film stability under harsh environmental conditions.

The thermocouple performance test was performed on the C type test coupon described in section IIB. The 10 cm long bar is inserted into a propane air torch flame to immerse the thermocouple junction while the thin film connections are made remote from the high temperature junction. A reference grade Pt-PtRh thermocouple is joined to the junction area of the bar to monitor the temperature for comparison.

F. Analytical Characterization Techniques

Analytical techniques have been applied to characterize various aspects of the layers, surfaces and interfaces present in the thin film thermocouple devices. The overall objective was to identify the most desirable methods for each fabrication step. Characterizations were carried out to document the quality of the insulating aluminum oxide layer, the degree of metal diffusion into the aluminum oxide, and the amount and type of near-surface impurities. The role of Al_2O_3 diffusion barriers was also investigated. Comparative studies were conducted on samples from all four classes (A-D) of substrates; these samples had been treated in different atmospheres at different temperatures, and had received different types of oxide coatings (thermal or rf sputtered) in an attempt to develop the best fabrication procedures.

The techniques used included scanning electron microscopy (SEM), energy dispersive x-ray analysis (EDX) and x-ray photoemission spectroscopy (XPS). These analysis methods were chosen since they can provide complementary information relating to the structure, composition and chemistry of interfacial regions. For example, SEM measurements give a direct picture of surface (or cross sectional) microstructure, while EDX can identify the composition of features seen within the SEM micrographs. While EDX has a relatively high lateral spatial resolution, its sampling depth is about 1 μm; XPS, on the other hand, has a nominal sampling depth of 5 nm, and can therefore provide key information about the composition at the surface of films used in the thermocouple devices. In addition, XPS can detect elements of low atomic number (like oxygen), which EDX cannot, and XPS also indicates the chemical environment in which the detected atoms exist.

1. SEM and EDX

SEM and EDX measurements were done using two separate commercial instruments each equipped with an electron microscope and integrated EDX capabilities. Samples were potted in epoxy either for viewing a face, or for cross-sectional cutting, polishing and viewing. Specimens were carbon- coated to reduce charging effects produced by the incident SEM electron beam. SEM was used to observe various structural features, including phase separations, and to position samples for EDX analysis. "Spot mode" EDX permitted the composition of different phases to be determined, and in the "integrated area mode" EDX was applied to obtain composition profiles across the oxide/coating and coating/substrate interfaces. In particular, a window of analysis was chosen for the EDX, that is an area at a specific magnification, so that analysis covered small changes in chemical composition. This was done for all heat treated materials and compared to a 'reference piece' of non-heat treated material. The results of the

analysis were all computerized using a standard- less semi-quantitative program of the EDX unit. Results compared favorable to the compositional values given for the 'reference' sample.

All SEM/EDX procedures were kept constant, i.e., KV, tilt, working distance, time of analysis, so that accurate comparisons could be made.

2. X-Ray Photoemission

Surface effects can play a critial role in the adherence and durability of thin overlayers. Therefore, x-ray photoemission spectroscopy was used to study the outermost layers of certain samples to evaluate the fabrication methods. Several brands of commercial spectrometers were utilized [Leybold-Heraeus (14), Physical Electronics (14) and Vacuum Generators (14)] during the course of this project. Samples to be investigated were placed "as is" into the ultrahigh vacuum enclosure of the photoelectron spectrometer, and lightly sputter-etched to obtain a "clean" surface.

XPS measurements allowed correlations to be made between fabrication conditions and the composition and chemical state of species produced at the surface of a variety of samples. The chemical composition of the surface region obtained from XPS data was used to identify impurities that might degrade adherence. XPS results were also used to detect oxide-stabilizing additives (like Y) as well as the presence of metal atoms which had segregated from the coating into the surface region of the insulating (thermal or sputtered) oxide layer. Since all elements except hydrogen can be detected in an XPS spectrum, the relative amounts of the different elements observed could be estimated and used to find stoichiometries of compounds at the specimen surface (e.g. x and y in Al_xO_y). In doing so, however, differing photoemission cross sections for the energy levels of the elements had to be accounted for.

Chemical shifts of the core electron levels were also used to obtain information on the bonding environment of a given type of atom in the surface region. In addition, the insulating quality of a poorly conducting layer could be inferred by the uniform charging-induced shift of all core levels from a sample which was losing photoelectrons without being completely neutralized.

III. RESULTS

A Substrate-Coating Stability

A series of the nickel blade alloy (MAR M200 + Hf) was coated with sputtered NiCoCrAlY. As mentioned above, considerable difficulty was encountered in obtaining test coupons with the barrier layer sputtered Al_2O_3 plus the NiCoCrAlY, but, three coupons were in the appropriate condition to study the effectiveness of the barrier coating in this system. Since the primary diffusion problem in this system is aluminum diffusion into the structural alloy MAR M200 + Hf, aluminum was the primary focus of the investigation. The samples included a comparison sample (D24) which had vendor sputtered Al_2O_3 approximately one μm in thickness and the standard vendor sputtered NiCoCrAlY (nominally 23% Co, 18% Cr, 12% Al and 0.5% Y). A second coupon (D4) was heat treated at 1090°C for fifty hours without the barrier layer also for comparison and the third coupon (D14) was heat treated at 1080°C for fifty hours with the 1.0 μm barrier layer to determine if the barrier layer would deter interdiffusion.

An electron scan of test coupon D24 is given in Fig. 6 in which the Al signal is highlighted on the electron dispersive X-ray analysis display. It is evident that the aluminum oxide is approximately 2 μm thick. This oxide is composed of thermal oxide generated by the vendor and sputtered oxide. The thermal

oxide presence is established by the aluminum depleted layer in the substrate immediately below the oxide. Data on the composition profile are presented in Table 3 and the comparisons to nominal composition indicate good agreement although the substrate evidently has considerable silicon. The low yttrium in the analysis may be inaccurate in our measurement, but was not considered important to the study. It can be inferred that the spot should be at least 3 m from the oxide to obtain unbiased readings.

Test coupon D4 was heat treated at 1090°C for 50 hrs without the barrier coating and a scanning electron micrograph is presented in Fig. 7. The white areas related to insulator charging and are not considered important. However, it is clear that oxides are not only forming on the surface but are penetrating into the coating. This is confirmed in the Al map of the same area of the coating (Fig. 8). Pettit has reported similar oxide growth and this may result from diffusion pipes or actual pores in the sputtered coating. This columnar structure of the coating is difficult to suppress at high sputtering deposition rates.

The diffusion profile of test coupon D4 is presented in Table 4 and Fig. 9. Because the Ni, Co, and Cr concentrations are similar in coating and the substrate, it is difficult to deduce any precise information. This problem is complicated by the two phase structure of both the coating (Fig. 2) and substrate alloys which partition Ni, Co, and Cr in slightly different amounts. That partitioning is evident in the Ni, Co, and Cr maps of both the coating and substrate and was a factor in the choice of spot size and location for the EDX analysis. The diffusion profiles of Ni, Co, and Cr indicate that Ni is entering the coating to make up approximately half of the difference between coating and substrate compositions. The penetration depth over which the Ni concentration increases significantly is probably 50-60 μm. Si and Ti appear to have little,

17

if any, mobility and that relates to the fact that they are undoubtedly tied up as oxides. The aluminum concentration is the primary species of interest. The expectations are that aluminum will be depleted near an oxidizing surface and that aluminum would move into the substrate from the higher aluminum containing coating. These tendencies are masked by inhomogenieties primarily caused by the formation of Al_2O_3 in the bulk phases.

The depletion of aluminum near the surface is evident in Fig. 9. Little aluminum penetration into the substrate is evident and that is probably a result of the vendor's heat treatment before coating which depletes the aluminum from the edge of the substrate (Fig. 6).

The test coupon D14 was obtained with a 1 μm Al_2O_3 barrier coating between the NiCoCrAlY and MAR M200 and heat treated 50 hrs at 1080°C. Figures 10, 11, 12 and 13 show the scanning electron micrograph, the Al map, the Co map, and the Cr map at 580x. The data from one of the diffusion profiles are presented in Table 5 and Fig. 14. The concentration 10 μm in from the edge indicates primarily the Al depletion due to oxidation. This is followed by a gradual build up of Ni which has come from the substrate and a Ni depleted area in the substrate near the Al_2O_3 barrier. This latter effect is related to the presence of Hf, Zr, Nb, Si, and Ti in that area as precipitates which results in depression of the Ni concentration. It may be that the EDX analysis is underreporting the Ni which reaches a level of 64% rather than 70% in the bulk at 200 μm distance from the edge. Co and Cr have diffused from the coating into the substrate primarily in the zone between 80 and 100 μm from the edge. This zone near the interface between the coating and substrate is a region of considerable phase transformations and because of uneven diffusion may even have voids. In this investigation with several samples, it almost appeared that the interface had moved as will be noted below. The Co and Cr concentrations show the

18

general movement out of the coating and into the substrate but the problem mentioned above in discussing D4 is also present. Aluminum concentration values again indicate the depletion near the surface and very little penetration into the substrate.

In summary, the NiCoCrAlY coating on the MAR M200 + Hf appears to be a well matched combination which, through consumption of aluminum by oxidation, prevents softening of the substrate from aluminum diffusion. The investigation of the barrier coating indicated little difference between the two coupons with and without the barrier coating. This difference is lessened by the similar compositions of coating and substrate and by the complexities of the two microstructures. It should be observed that the commercial application is planned without a barrier layer.

The barrier layer is much more important in the systems employing FeCrAlY as the coating material. Both aluminum and iron can diffuse into the substrate and lower the creep strength. For this investigation, the combination of FeCrAlY plus MAR M509 was chosen because the contrast in compositions would more clearly delineate the diffusion profiles and the high temperatures of the vane alloy in service. The aluminum oxide barrier layer was sputtered on by the vendor prior to the sputtered FeCrAlY. Two temperatures, 1125°C and 1075°C, were used to heat treat both 0.6 μm and 2 μm thickness barrier layers. Delamination of the coating at the barrier layer was a serious problem and the principal data was obtained from samples A62 which was not heat treated, A40 which had no barrier layer and was heat treated 50 hours at 1075°C, and A19 which had 2 m of Al_2O_3 and was heat treated 86 hrs at 1075°C. The same procedures were followed as with the "D" coupons which were described above.

Test coupon A62, the comparison test coupon, was used to confirm the technique and explore any unusual conditions that might complicate the procedure.

The Al_2O_3 appeared to be uneven in the SEM images and the Al_2O_3 was damaged in the sample preparation so that it was difficult to tell if the layer had perfect continuity. The EDX results are reported in Table 6. The small spot size 1x1 µm tends to pick out inhomogenieties particularly in the two phase structures. No quantitative analysis was recorded for the tungsten, tantalum, titanium, or zirconium in the substrate alloy since the principal interest in this study was to follow iron and aluminum penetration into the cobalt alloy. The low value of aluminum in the coating may have resulted from losses in the sputtering process or the lower yield of aluminum compared to that of iron. The complexity of the cobalt alloy is evident by the variability of the Co and Cr contents.

Test coupon A40 was heat treated at 1075°C for 50 hours without the barrier coating to determine the diffusion profiles. The results of the EDX investigation are presented in Table 7. Figure 15 and 16 are typical diagrams of counts versus energy from which the data are generated. Fig. 15 is at point 10 in the substrate material 113 µm from the edge of the sample. The diffusion profiles of Fe, Al, Cr, and Co are plotted in Fig. 17. It is evident that Co diffuses rapidly through the 80 µm of the b.c.c. FeCrAlY coating and reaches a 25% weight fraction all the way to the edge. The aluminum concentration is well below 1% only 30 µm from the interface between the coating and substrate indicating that even without the barrier aluminum diffusion is not a serious problem. These results correspond with the previously reported results (9) of the NiCoCrAlY/MAR M200 + Hf system. Iron penetration is not very severe after 50 hours at 1075°C reaching less than one quarter of its concentration 10-12 µm from the barrier and showing vanishingly small concentrations at 30 µm (Fig. 17).

Test coupon A19 was heat treated at 1075°C for 86 hours with a 2 µm Al_2O_3 barrier layer. The longer heat treatment yields a "go-no go" test;

20

that is, if the iron and aluminum penetration are not significantly less the barrier coating is not working. A scanning electron micrograph is presented in Fig. 18. The photograph at 1000X indicates some damage to the FeCrAlY coating at the interface, but perhaps more significantly it appears that metal bridges are formed through the Al_2O_3 barrier layer. The diffusion data is presented in Table 8 and a second profile in Table 9. The data from Table 8 are also presented in Fig. 19. Again, the cobalt is rapidly diffusing through the FeCrAlY reaching approximately 25% by weight in the b.c.c. phase. The iron concentration is penetrating at approximately 40 μm to quarter of peak height. This is a greater amount than the diffusion in the A40 coupon which had no barrier. Aluminum penetration to quarter height is also approximately 40 μm. It is clear that the Al_2O_3 barrier is not preventing (or slowing down) diffusion of iron or aluminum into the substrate and it is not slowing down cobalt diffusion into the coating. Chromium is probably not a problem in these alloys. The indications are that the coating is being breached by cracks or holes and the impermeability of the Al_2O_3 for Al, Fe, and Co is not being utilized. Perhaps an improvement of the Al_2O_3 coating technique (for both bonding and continuity) coupled with a rigorous inspection technique could yield a useful barrier layer.

B. Dielectric Strength and Adhesion

1. Thermal Oxidation

Thermal oxidation of the MCrAlY coatings is a critical step in the creation of a durable, adherent, insulating layer between the turbine engine hardware and the thin film thermocouple sensor. As was discussed in Section II, Experimental

Materials and Methods, considerable research has lead to the technology of the MCrAlY coatings and the protective oxide. In order to optimize the oxide for the insulating layer, considerable care must be taken to obtain a uniform, continuous Al_2O_3 base for the sputtered Al_2O_3 film. Selective oxidation has been used to suppress the formation of nickel, cobalt, and iron oxides which have poorer electrical properties and may lead to spinels and other second phases which would disturb the continuity of the oxide film and weaken its resistance to cracking during thermal cycling. This investigation studies the effects of oxidation under various oxygen partial pressures and temperatures on various FeCrAlY and NiCoCrAlY coatings.

The FeCrAlY - MAR M509 system had been recommended because it forms "forgiving" oxide; however, in order to obtain good adherence of the sputtered layers, a certain degree of surface roughness was recommended. It was found that too rough a surface would lead to uneven oxide growth. Test coupon A4 (Fig. 20) had a 400 mesh final surface preparation and yielded oxide channeling as depicted in the figure; therefore, all subsequent samples were given a 600 mesh finish. The need for surface removal is made clear in Fig. 4 where the uneven FeCrAlY surface is clear. The dark area in the figure is FeCrAlY with the metal substrate below and a nickel plating to protect the faceted FeCrAlY coating. The columnar nature of the sputtered coating is evident in the photograph. The FeCrAlY coating also had a tendency to form pits below the oxide film especially when the oxide was grown in air. Fig. 21 illustrates this problem; the oxide film has cracked and spalled revealing the pitting surface underneath. The pitting is probably a result of excessive aluminum loss from specific locations. The sample A35 in Fig. 21 was oxidized in dry argon ($H_2O>10$ ppm) for 13 hours at 1070°C followed by 49 hours in air at 1070°C. Samples without the low oxygen partial pressures in the early stages were generally

22

worse and samples oxidized at temperatures, i.e., 1120°C were severely spalled and contained black oxides. A complete oxide film could be obtained under the conditions used for sample A42A, (1050°C for 80 hours in wet argon) and for sample A43A (1080°C for 50 hrs in dry argon). A42A had an oxide thickness calculated from its weight gain of 1.6 μm and A43A had a thickness of 1.9 μm. A photomicrograph of sample A43A is shown with the sputtered coating in the next section.

FeCrAlY coatings on MAR M200 + Hf had similar problems and thermal oxide thicknesses are presented in Table 11. Fig. 22 illustrates a second problem on sample B10 which was exposed at 1090°C for 66 hours in an argon plus 4% H_2 atmosphere. Here the Al_2O_3 growth habit is not only in a film but generates "leaders" of more rapidly growing oxide in mounds. The average thickness of this oxide was calculated to be 1.6 μm. Adequate film growth was obtained under the conditions used for sample B41 shown in Fig. 23 (13 hours in dry argon plus 49 hours in air, both at 1070°C). This oxide was 2.1 μm thick.

Fewer problems were encountered with MAR M200 + Hf plus the electron beam deposited NiCoCrAlY system. A cross section of the sputtered NiCoCrAlY coating was given in Fig. 2. The two phase coating has a smoother surface (top dark line). Typically, the oxide appeared as in Fig. 24 with a fairly smooth scale plus small Al_2O_3 needles. This coupon is sample C21 heat treated at 1075°C for 16 hours in argon and 33 hours in air, resulting in approximately 2 μm of oxide scale. Poor results were obtained at 1120°C where green oxide seemed to break through the scale and disrupt the continuity. Similarly, the sputtered NiCoCrAlY on MAR M 200 + Hf generated a good oxide. Sample D8 (Fig. 25) was heat treated under the same conditions as C21 (1075°C for 13 hrs in Ar, 33 hrs in air) and also displayed the Al_2O_3 needles. Smeggil and Bornstein[25] have related the needle habit of Al_2O_3 on NiAl to the presence of 0.61 ppm NaCl.

23

For thermal oxide layers, different growth atmospheres and oxidizing temperatures were investigated analytically. In general, the substrate was not found to have a significant effect on the oxide obtained, but some differences were observed for the oxide grown on the FeCrAlY and NiCoCrAlY coatings. EDX measurements on both FeCrAlY-based oxides (like C26 [Ar+3%H_2O oxidized, 1050°C]) indicated that metals from the coating diffused into the thermal oxide during heating. The nominal 1 m depth of the EDX technique meant that significant amounts of metals like Fe and Ni, Cr and Co had diffused to within 1 m of the surface, but no conclusive statement could be made about the important region just below the oxide surface.

XPS measurements, however, with their higher surface sensitivity, showed that these metals did diffuse to within 5 nm of the oxide surface. The FeCrAlY-coated sample A42 [air oxidized, 1075°C] had Fe and Cr levels near 0.1 atomic percent in its oxide layer, while NiCoCrAlY-coated C12 [Ar+H_2O oxidized at 1090°C] had Ni and Cr (and presumably Co, which was not recorded) in its oxide at about 0.5 atomic percent. The C12 sample also appeared to have a surface enrichment of yttrium, apparently due to the diffusion of Y to surfaces where it reacted with oxygen. The yttrium effect was noted in other thermally treated samples as well.

Various impurities were also observed in the XPS spectra of many of the samples analyzed. Although carbon levels were sometimes quite high, it is believed that much of the carbon collected on the surfaces during post-oxidation handling. Other impurities, like Si and As, at levels of approximately 2.5 and 0.5 atomic percent, were also observed. Si is an impurity that has been identified by the substrate/coating vendor.

The key role to be played by the oxide layer on these samples is as electrical insulation. This property could be monitored using resistivity

measurements, but the core level shifts of the XPS peaks were also found to provide a useful diagnostic of the insulating quality of these oxide layers. Core level shifts can occur either due to chemical factors, or because of surface charging. The latter effect produces a uniform shift to higher binding energy for all recorded XPS features. Insulating qualities determined from observed charging shifts were generally in agreement with available resistivity measurements.

Charging shifts for thermally oxidized samples were always smaller than those observed from sputtered layers of aluminum oxide over a thermal oxide. For example, Figure 26 illustrates an approximately 6 eV shift (mainly from charging since both surfaces are predominantly aluminum oxide) between the oxygen 1s electrons emitted from the sputtered oxide on C14 (2.8 µm sputtered over 2.7 µm thermal) and the Ar+H_2O-grown oxide on C12 (1.1 µm). In this case, the difference in the thicknesses may explain at least part of the larger shift for C14. Charging shifts for air-oxidized samples like A42 [1075°C], B23 [1077°C] and D2 [1025°C] were usually intermediate between the sputtered and Ar+H_2O grown oxides (1.5 eV or more above the Ar+H_2O oxides, and about 1.5 eV below the sputtered overlayer). The charging shift in Figure 27 shows that the air-oxidized D2 (2.7 µm) has a better insulating layer than D1 (Ar+H_2O, 2.6 µm) even though these layers have essentially the same thickness. Notice that there is some difference in the O1s position for the Ar+H_2O oxidized samples C12 [1090°C] and D1 [1050°C] in Figures 26 and 27. This difference, as well as the generally poorer insulating quality of the thermally grown oxides may be connected, not only to differences in oxide thickness, but also to the presence of pores and pits that have been optically observed in such layers. It is possible that the sputtered layers fill these pores, thereby leading to the larger charging shifts that are indicative of better insulating layers.

It is interesting to note also that the Ar+H$_2$O grown oxides may have a somewhat higher Ni and Cr content than their air-grown analogues. Figure 28 shows what is probably the strongest Ni core level signals observed during this study from an aluminum oxide, in this case a Ar+H$_2$O-grown layer on sample D1. A feature attributable to nickel oxide is also observed several electron volts higher in binding energy. The metallic Ni peak would indicate that the Ni oxidation reaction did not go to completion in the Ar+H$_2$O atmosphere.

Despite some presence of nickel, chromium and cobalt oxides and yttrium oxide in almost all the thermally grown layers, the insulating oxide was predominantly (typically $\geq$ 95%) aluminum oxide. Quantitative evaluations of elemental concentrations were obtained using XPS peak areas, and accounting for core level dependent photoemission cross sections and instrument transmission functions. The aluminum to oxygen ratio was generally close to 2:3 when corrected (see Figure 29), indicating stoichiometric Al$_2$O$_3$ at the surface (e.g. A63 [air, 1025°C], B23 [air, 1075°C]); however, certain samples seemed to be somewhat oxygen rich at the surface (e.g. A42 [air, 1075°C], B38 [Ar+H$_2$O, 1065°C]).

The principal tests for thermal oxide on both the FeCrAlY and NiCoCrAlY coatings were appearance (no color) and electrical impedance. The latter test was conducted by containing the sample in two drops of moisture with two probes to insure at least one megaohm d.c. resistance. The oxide was also scratched and observed in a light microscope. Indications were that no preference could be ascertained related to the use of argon with 4% H$_2$ which suppresses the formation of chromium oxides. The NiCoCrAlY coatings seemed to generate good thermal oxides using both argon followed by air oxidation and using air oxidation. FeCrAlY (18:11:1) was more troublesome with the generation of the pits and oxide spalling but adequate oxides could be obtained by starting with an

argon atmosphere. Spalling was a more serious problem with thicker 2 m oxide scales.

2. Sputtered Thin Films

The thin film thermocouples are composed of various layers approximately 1-2 μm thick. Their electrical performance requires an insulator of high dielectric performance to prevent breakdown and high resistance ($>$10kΩ) over distances of approximately 2 μm. Therefore, the insulator must be pore free and free of 2 μm diameter defects that would affect the electrical properties. As was mentioned in the Introduction, aluminum oxide is an excellent choice for the insulator and reactive vacuum sputtering has been found to be a useful way of achieving these properties. Similarly, the platinum and platinum-rhodium alloy films must have excellent electrical properties. Thin film deposition of platinum group metals can be achieved by numerous means such as electroplating, electron beam coating, slurry and sinter techniques, electrophoresis, electroless deposition, etc., but the sputtering technique has been found by the electronics industry to be preferred. The metal films of the thermocouple must be uniform, strong, ductile, adherent, stable, and durable. The sputtering technique has been used in the aircraft engine industry and can be commercialized with confidence because of its use by many vendors in the electronics industry.

Reactive sputtering of aluminum oxide has been described by Berry[26], Thornton[27,28], Schwartz[29], Maissel[30], Waits[31], Urbanek[32], and Nowicki[33]. The development of RF sputtering enabled the production of non-metallic films leading to unique capabilities of this technique. The Al_2O_3 sputtered film can be produced using an aluminum target or an alumina target since the RF field does not require a conducting target. Since the bombarding species is almost completely of atomic form both targets are similar in

practice. To achieve Al_2O_3 in the substrate film oxygen must be present in the sputtering atmosphere which reacts with the deposited film as it is built up. In fact, with oxygen present in the sputtering atmosphere, an aluminum target is rapidly oxidized so that both aluminum and alumina targets have similar surfaces. Aluminum targets are to be preferred because of the ease of fabrication and superior heat transfer characteristics.

The technique for deposition of the Al_2O_3 insulating film was planar magetron DC sputtering. This technique was pioneered by Nowicki[33] at Honeywell for MOS devices and is superior to CVD because of the better control of residual stresses. The magnetron has the added advantage of high deposition rates and therefore greater promise as a commercial technique. In this investigation, 1100 aluminum was used in preference to the 6061 alloy used by Nowicki to avoid contamination by silicon and magnesium. The presence of magnesium, however, may promote better adhesion (34,35).

Experimental investigations of sputtering rates, atmospheres, target to substrate distances, and power levels were used to optimize coating purity, smoothness, and adhesion. Purity is verified by optical clarity and absences of color. Smoothness is verified with the optical microscope, and adhesion was measured with a Sebastian adhesion tester. The best quality films were produced using 250-300 watts on a 5 cm diameter target of 1100 aluminum at 15 cm target to substrate distance. The pressure of the sputtering atmosphere of 90% argon, 10% oxygen, was 2×10^2 Pa to optimize the film. Typical sputtering rates were 0.2-0.3 nm per second so that a 1 μm film required three hours to deposit. Typical good sputtered films are shown in Figs. 30 and 31. Test coupon A43A in Fig. 30 has 2.6 μm of sputtered Al_2O_3 and C19 has 1.9 μm. At 500X, the coating is colorless, clear, and appears to have 1-2 μm hills which are a reproduction of the thermal oxide topography. Each coating is made on a glass slide

as well as the test coupon. The coatings on the glass slide were used to evaluate the clarity, thickness, and smoothness.

Thickness of the coating is an important parameter and three methods were used for its measurement. During the coating, the rate and accumulation are measured using a calibrated quartz oscillating crystal. Weight gain was measured on each sample and glass slide. The weight gain was calculated using estimates of the covered area and some allowance had to be made for wrap around coating on unmasked areas. The weight gain estimate of thickness is probably within 10% of the true value. The third method employed a Leitz (14) optical interferometer. Typical interferometric measurements are shown in Fig. 32 indicating 1.6 and 1.9 μm, respectively. The technique used thallium radiation with a 0.27 μm wavelength which is appropriate for films 1-2 μm in thickness. The photographs indicate the step height from masked to unmasked areas of the glass slide. Assumptions of thickness uniformity are based primarily on manufacturers specifications relating the target to substrate geometries. The best interferometric examination of Al_2O_3 films confirmed the absence of any major deviations on areas 10x2.5 cm of the glass slide. Although the thickness measurements are given with two significant figures throughout the report, the best estimate of accuracy would be ±10%. Some thickness measurements are reported with one significant figure and the experimental accuracy for these measurements is not estimated to be within the ±10%. The adhesion properties of the Al_2O_3 and metal films are reported in the next section.

Analytical studies were also made of sputtered oxide layers. Even though thermal oxidation did not produce high quality insulating layers, it was found that the thermal oxide served as a good base for a reactively sputtered oxide overlayer. All sputtered aluminum oxides examined by XPS were deposited on a thermally grown oxide layer, and the XPS charging shifts indicated that such

sputtered oxide surfaces were consistently less conductive than thermal oxide surfaces as discussed above in reference to Figure 26.

Sample C14 is representative of specimens with a highly insulating layer consisting of both thermal and sputtered oxides. Although carbon was observed at the surface of this sample, the only other elements observed were aluminum and oxygen; other possible components, like Ni, Co, Cr or Si (see above) were not present at levels that could be observed, if they were present at all. Figures 33 and 34 compare spectra of the Ni and Cr 2p regions of the C14 sputtered oxide surface with those from an $Ar+H_2O$ grown oxide surface (C12). The lower surface conductivity of C14 could have been due in part to the absence of any Ni, Cr or Co oxides in such specimens. These species are much less likely to diffuse up into the sputtered oxide layer at the relatively low temperatures the samples reach during sputter deposition.

Platinum and platinum-10% rhodium films for the thermocouples were also deposited using planar magnetron vacuum sputtering. The best films were made using a target to substrate distance of 15-20 cm, 200-250 watts, 0.14 Pa argon sputtering gas and electrically grounded substrates. The target materials were case pure 10 cm discs approximately 0.3 cm in thickness. The deposition rates were approximately 0.6-0.8 nm per second and no significant difficulties were encountered in obtaining good quality coatings which were generally mirror smooth on the glass slide and reproduced the surface topography of the test coupon. Adhesion and durability of these coatings is discussed below.

The masking for the thermocouple pattern was accomplished using 0.12 mm thick steel shim stock. This material is easy to cut and provided the necessary resolution for the thermocouple patterns required. Simple spring clamps could be used to provide masking for thermocouple legs of 1 mm width. The small test coupon with a sputtered thermocouple pattern is shown in Fig. 35 and the long

30

thermocouple test coupon is shown in Fig. 36. Typical thicknesses deposited for the platinum and platinum-rhodium were 1-2 μm.

3. Sputtered Coating Adhesion and Thermal-Mechanical Performance

One of the critical properties of the thin film thermocouple relates to its adhesion and stability on the substrate. As was described in earlier sections the tests used to verify this integrity include thermal cycling and adherence testing of the sputtered oxide and platinum alloy films. The results of these tests are presented in Tables 10, 11, 12 and 13 for each of the material systems.

Table 10 is a summary of the heat treatments, thicknesses and adhesion strength of the thin film sensor samples fabricated on the MAR M509 plus FeCrAlY. The system heat treatments were made at temperatures ranging from 1025 to 1120°C but the highest temperature used successfully was 1090°C. In order to obtain 1.5 μm thickness of thermal oxide in approximately 50 hrs, temperatures of over 1075°C were required with dry Argon (less than 10 ppm oxygen); even 1090°C was not adequate for 66 hours in argon plus hydrogen. Air or argon plus 3% H_2O atmospheres lead to adequate (1.5 μm) oxides at 1050°C and above after 50 hours. Adhesion of the sputtered oxide was not a serious problem in any of the tests (A4, A15, A43, and A43A). The adherence of the platinum film was a problem on A4 which had the rough thermal oxide (Fig. 20). The dark sputtered oxide on samples A62 and A63 probably relates to metallic contamination of the coating and these samples were note tested.

Table 11 is a summary of the heat treatments, oxide thicknesses, and adhesion strengths of the thin films of the MAR M200+Hf plus FeCrAlY system (B). Results on oxide thickness similar to those observed on the "A" samples would lead to recommendations of temperatures of 1050-1090°C for 50 hours in air or

31

argon plus H_2O at the dew point (~3% H_2O). Again, the sputtered oxide adherence was high (B16, B27A, B41, B45, B47, B49). The platinum adherence was also good on B16 and B47. Sample B49 had poor platinum adherence and also had a rough thermal oxide. Photo-micrographs of B49 indicate some spalling of the thermal oxide which may have related to contamination of the surface.

Table 12 summarizes the heat treatments, oxide thicknesses, and adhesion strengths of the thin films on the MAR M200+Hf plus NiCoCrAlY (electron beam deposited) samples. Again, it was difficult to achieve adequate thickness of thermal oxide in dry argon or argon plus 4% hydrogen at temperatures below 1100°C. Generally, the thermal oxides were thicker and smoother than those on the FeCrAlY. Adherence of sputtered oxide was good on all samples tested (C12, C13, C14, C15, C19, C20, C23, C24, C28) except C22 which had a thin oxide grown in dry argon. Adherence of the platinum films was good on C19, C20 and C24. These samples had thermal oxides matured in air. C12 had poor platinum film adherence.

Table 13 summarizes the heat treatments, oxide thickness and sputtered film adherence for the "D" samples of MAR M200+Hf plus NiCoCrAlY (sputtered). The thermal oxide was generally darker than those oxides deposited by the electron beam method. Deposited NiCoCrAlY samples and some "D" samples had a blue oxide contamination eminating from the uncoated edges. Samples with non-chromatic oxides had good sputter film adherence.

In order to evaluate the adherence of the platinum-platinum 10% rhodium films, thermal cycling tests were used. The test coupons weigh approximately 10 grams and are approximately 0.8 cm thick. They have 70-100 μm of NiCoCrAlY or FeCrAlY plus 1-2 μm thermal oxide and 1-2 μm sputtered aluminum oxide under the 2 μm thermocouple film. Each coupon was heated with a torch to 1000°C in 60-90 sec and cooled in air to 500°C, then water quenched to below 100°C and recycled.

The tests included eight cycles for each sample. Temperatures were measured with a type S thermocouple in an Al_2O_3 tube between the base of the specimen and a refractory brick. The surface temperature of the sample was also monitored with a L&N disappearing filament pyrometer. The peak temperature recorded is conservative since emissivity corrections were not made and the thermocouple is not directly exposed to the flame. In fact, certain portions of the film were obviously hotter. The thermal cycling did produce defects in the platinum and platinum-rhodium films which were apparent under the microscope and lead to microscopic rupture in one sample (B16). The defects appeared in photo-micrographs as small blisters 10-100 μm in diameter which are expanded probably due to excessive overheating and plastic deformation at peak temperatures and lack of good adhesion or thermal contact. Both B16 (FeCrAlY on MAR M200) and C24 (NiCoCrAlY on MAR M200) demonstrated this behavior. A40 (FeCrAlY on MAR M509) did not have the blisters, but the oxide on this specimen was rough.

4. Electrical Performance

The electrical performance of all four types of test coupons (A, B, C, and D) were evaluated. In fact, all sputtered oxide and thermal oxide films were checked at room temperature by direct contact with an ohmmeter probe capable of measuring up to two megahoms. The area of the film under the ohmic probe was wet with tap water (200-500 K ohms at 1 cm) to connect any pores with the probe. Thermal oxide films such as C11, A38, and B23 which were overheated did not pass this test and were not sputter coated. The high temperature electrical test was made on the fixture described in Section IIE (Fig. 5) and permitted monitoring electrical resistance between the platinum thin film and the substrate, along approximately 1.5 cm of length of the bimetallic film, or between two points on the oxide 1.5 cm apart. Typical results of testing A, B, C, and D type

sputtered oxide films are presented in Fig. 37. The oxide films on NiCoCrAlY (type C and D) had resistance values greater than two megohms below about 900°C but the resistance fell rapidly to several·hundred kiloohms at temperatures above 1050°C. The steep decreasing slope in oxide resistance with increasing temperature is comparable to those given in Samsanov[36],[37]. The data indicate decreases from $4x10^8$ ohms at 600°C to $3.5x10^6$ at 800°C to $5x10^4$ at 1000°C and $1x10^4$ at 1100°C for sintered aluminum oxide and similar decreases occur for single crystals. This very steep slope of one to two decades per 100°C in the critical range strongly indicates the need for high temperature testing. The oxide films on FeCrAlY were apparently actively growing above 700°C because of the increase in resistance measured at 800°C region (Fig. 37). Generally, the resistance of these films was not as great as those formed on NiCoCrAlY. The test fixture also permitted evaluation of dielectric breakdown. A one volt potential was placed over the 2-4 µm thick oxide film at each temperature up to the maximum temperature but no dielectric breakdown was observed on any test sample. The high dielectric strength of Al_2O_3 is no doubt adequate for thermocouple voltages and even for thin film strain gages with similar dimensions.

Tests on the platinum-platinum rhodium alloy films were conducted with the same equipment. In addition to measuring the resistance to ground, a continuous measurement of the metallic thin film resistance was made. Samples A43A, C19, D4 and D5 also were fabricated with thicker oxide layers than A40, B16, C24, and D2 to improve the high temperature performance. In fact, all four test coupons had greater than two megohms resistance between ground and the platinum at the following test temperatures: 970°C for A43A, 960°C for D4, 1080°C for D5, and 1120°C for C19. The C19 test coupon was taken to 1169°C where the resistance

fell to 350 K ohms. The platinum alloy bimetallic strip increased in resistance at high temperatures as expected.

Full size thin film thermocouple test specimens shown in Fig. 36, were tested for thermocouple output. This specimen which is over 10 cm long permitted testing in a propane torch on one end while maintaining the cold end near room temperature. Type S reference grade thermocouples (250 μm diameter) were fixed to each end of the 10 cm bar during heating to monitor metal temperatures. Although this test was not sufficiently precise to be considered a calibration, it was used to determine that the thermocouple was indeed working properly. Sample C31 thin film thermocouple test coupon followed the output of the attached thermocouple. Some difficulties were encountered in maintaining the attached thermocouple in intimate contact with the test bar above 900°C in the flame so that stability measurements were not possible with this arrangement.

The same thin film thermocouple bar, C31, was inserted through the wall of a silicon carbide rod heated furnace to obtain long time stability information. The refractory wall of the furnace was 9 cm thick leaving approximatley 0.5 cm extension of the junction into the furnace and 0.5 cm for connections outside outside the furnace. Both ends were monitored with Pt-Pt 10% Rh thermocouples touching the MAR M200 bar. The heat transfer along the bar lead to intermediate values of thermocouple output voltages on the thin film thermocouple compared to the thermocouples used for monitoring. For example, the monitors read 0.99 mv (165°C) and 9.13 mv (975°C) on the outboard and inboard points respectively when the thin film thermocouple was reading only 6.36 (725°C).

This severe temperature gradient along the test bar may have contributed to a failure in the form of an open circuit at approximately 10 hours. The platinum leg had debonded from the test bar which terminated the test. The results of these thin film thermocouple tests indicated the general validity of the

fabrication method but are not considered a good simulation of true engine test conditions. These tests should be conducted by engine manufacturers where the complex geometries and application conditions can be used.

REFERENCES

1. Burger, H.C. and Van Citter, P.H., "Preparation of Bismuth-Antimony Vacuum Thermal Elements by Vaporization", Z. Phys., Vol. 66, 1930, p. 210.

2. Harris, L., and Johnson, E.A., "Technique of Sputtering Sensitive Thermocouples", Rev. Sci. Inst. 5, 1934, p. 153.

3. Chopra, K.L., Thin Film Phenomena, McGraw Hill, New York, 1969.

4. Dils, R.R., "Process of Coating a Gas Turbine Engine Alloy Substrate", U.S. Patent 3, 890, 456, 17 June 1975.

5. Dils, R.R. and Follansbee, P.S., "Superalloy Sensor", Superalloys: Metallurgy and Manufacture, Kear, B.H., Muzyka, D.R., Tien, J.K., and Wlodek, S.T., Eds., Claitor, Baton Rouge, La., 1976, pp. 37-44.

6. Grant, H.P. and Przybyszewski, J.S., "Heat Transfer Coefficients Around Cylinders in Crossflow in Combustor Exhaust Gases", JOURNAL OF ENGINEERING FOR POWER, TRANS, ASME, 99, No. 4, p. 497, 1977.

7. Grant, H.P., and Przybyszewski, J.S., "Thin Film Temperature Sensor", NASA CR-159782, Feb. 15, 1980.

8. Grant, H.P., Przybyszewski, J.S., and Claing, R.G., "Turbine Blade Temperature Measurements Using Thin Film Temperature Sensors", NASA CR-165201, March 17, 1981.

9. Grant, H.P., et al., "Thin Film Temperature Sensors Phase III", NASA CR-165476, Jan. 11, 1982.

10. Dils, R.R. and Follansbee, P.S., "Electronic and Ionic Conduction in Aluminum Oxides Grown on High Temperature Metal Alloys", presented at Symposium on High Temperature Electron and Ion Transport in Solids, Electrochemical Society Meeting, San Francisco, May 12-17, 1974.

11. Wells, C.H., Follansbee, P.S. and Dils, R.R., "Mechanisms of Dynamics Degradation of Surface Oxides", Stress Effects and Oxidation of Metals, J.V. Cathcart, Ed., AIME, New York, 1975, pp. 220-244.

12. Dils, R.R. and Follansbee, P.S., "Dynamic Oxidation and Corrosion in Power Generating Units", CORROSION, 33, No. 11, p. 385, 1977.

13. Dils, R.R., "Dynamic Gas Temperature Measurements in a Gas Turbine Transition Duct Exit", Journal of Engineering for Power, Trans. ASME, Vol. 95, Series A, No. 3, July 1973, p. 265.

14. Certain commercial equipment, instruments, and materials are identified in this paper in order to specify adequately the experimental procedure. In no case does such identification imply recommendation or endorsement by the National Bureau of Standards, nor does it imply that the material or equipment is necessarily the best available for the purpose.

15. T.K. Redden, "Ni-Al Coating-Base Metal Interactions in Several Nickel-Base Alloys", Trans. Metalurgical Society of AIME, Vol. 242, p. 1695, August 1968.

16. G.W. Goward, D.H. Boone and C.S. Giggins, "Formation and Degradation Mechanisms of Aluminide Coatings on Nickel-Base Superalloys", Tran. of ASM, Vol. 60, p. 228, 1967.

17. F.S. Pettit, "Oxidation Mechanisms for Nickel-Aluminum Alloys at Temperatures Between 900° and 1300°C", Trans. Metallurgical Society of AIME, Vol. 239, p. 1296, September 1967.

18. E.A. Gulbransen and K.F. Andrew, "Oxidation Studies on the Iron-Chromium-Aluminum Heater Alloys", J. Electrochemical Society, p. 294, April 1959.

19. G.W. Goward, "Current Research on the Surface Protection of Superalloys for Gas Turbine Engines", J. of Metals, p. 31, October 1970.

20. W.C. Hagel, "The Oxidation of Iron, Nickel and Cobalt-Base Alloys Containing Aluminum", Corrosion - Nat'l Assoc. of Corrosion, Engineers, Vol. 21, p. 317, October 1965.

21. C.S. Giggins and F.S. Pettit, "Oxidation of Ni-Cr Alloys Between 800° and 1200°C", Trans. Metallurgical Society of AIME, Vol. 245, p. 2495, December 1969.

22. W.E. Boggs, "The Oxidation of Iron-Aluminum Alloys from 450° to 900°C", J. Electrochem, Soc.: Solid State Science, p. 906, June 1971.

23. R.E. Grace and A.U. Seybolt, "Selective Oxidation of Al from an Al-Fe Alloy", J. Electrochemical Society, p. 582, October 1958.

24. J. Stringer, P.S. Corkish and D.P. Whittle, "Oxidation of Two-Phase Alloys", in Stress Effects and the Oxidation of Metals, J.V. Cathcart, Editor, Proc. Symp. 1974 TMS-AIME Fall Meeting, Oct. 21-24, 1974, Materials Science Symposium, publication of the Metallurgical Society of AIME, 1975.

25. Smeggil, N. Borstein, "The Effect of NaClCg on Oxidation of NiAl", J. Electrochem. Soc., Solid State Science and Technology, p. 1283, Aug. 1978.

26. Berry, R.W., P.M. Hall, and M.T. Harris, Thin Film Technology, Chapter 4, Van Nostrand, New York, 1968.

27. Thornton, J.A. and A.S. Penford from Thin Film Processes, J.L. Vossen and W. Kern, Academic Press, New York, 1978, p. 76-115.

28. Thornton, J.A. and V.L. Hedcoth, J. Vac. Sci., Tech. 13, 117 (1976).

29. Schwartz, N. Trans. 10th Nat. Vac Symposium, 1963, MacMillan, New York, p. 325 (1964).

30. Maissel, L.I., Physics of Thin Films. Vol. III, Academic Press, New York (1966).

31. R.K. Waits, Thin Film Processes, J.L. Vossen and W. Kern, Academic Press, New York, pp. 131-175 (1978).

32. Urbanek, K., "Solid State Tech", 20(4), 87 (1977).

33. Nowicki, R.S., J. Vac. Sci. Tech., Vol. 14, No. 1, p. 127 (Jan/Feb 1977).

34. Breinan, E.M., and K.G. Kreider, "Braze Bonding and Joining of Aluminum Boron Composities", Metal Engineering Quarterly, ASM, p. 5 (Nov. 1969).

35. Kreider, K.G., and K.M. Prewo, "Boron Aluminum Composites" in Metallic Matrix Composites, K.G. Kreider, Ed. Academic Press, New York (1974).

36. Samsonov, G.S., The Oxide Handbook, Trans. CN Turton, NY IFI/Plenum (1973).

37. Pentecost, J.L. Ceramic Age 71:26 (1958).

List of Tables

List of Illustrations

Table 1
Alloy Compositions
in weight %

Alloy					
MAR M200+Hf	Ni	10Co	9Cr	5Al	2Ti
		2Hf	1Cb	0.15B	0.14C
MAR M509	Co	24Cr	10Ni	7W	3.5Ta
		0.2Ti	0.5Zr	0.6C	
FeCrAlY	Fe	18Cr	11Al	0.7Y	
NiCoCrAlY	Ni	23Co	18Cr	12Al	0.5Y

Table 2
Material Systems and Designations

Substrate	Coating	Process	Designation
MAR M509	FeCrAlY	DC Sputtering	A
MAR M200+Hf	FeCrAlY	DC Sputtering	B
MAR M200+Hf	NiCoCrAlY	Electron Beam	C
MAR M200+Hf	NiCoCrAlY	DC Sputtering	D

Table 3
D24 Composition Profile - No Heat Treatment
(in weight percent)

	Nominal Coating	-5	-3	-1	1	3	5	Nominal Substrate
			Distance from barrier (in μm)					
Ni	54	55	55	48	56	63	64	71
Co	17	16	17	16	11	14	13	10
Cr	19	18	16	18	11	10	11	9
Al	12	11	11	18	14	5.3	5.3	5
Si	0	0.6	0.7	-	5.3	5.9	5.5	-
Ti	-	-	-	-	1.8	2.1	2.1	2

Table 4
D4 Composition Profiles - No Barrier
(in weight percent)

Distance from edge (in μm)

	0	10	20	30	40	70	80	90	100	120	140	150	200
Ni		51	56	62	56	65	64	66	66	68	66	68	66
Al	100	4	6.4	9.6	5.6	4.0	3.5	3.5	3.5	2.9	3.4	3.5	3.5
Si	0	0.9	0	0	0.8	3.7	5.8	5.7	5.7	5.2	4.5	4.2	5.4
Cr	0	23	19	13	18	10	12	10	11	10	12	10	11
Co	0	22	19	16	20	15	13	12	13	12	13	12	12
Ti	0	-	-	-	-	1.6	2.0	2.0	1.5	1.7	2.0	2.1	2.3

Table 5
D14 Composition Profile with Barrier
(in weight percent)

Distance from edge (in μm)

	10	20	30	40	50	60	70	80	90	100	110	120	130	140	150	200
Ni	50	53	54	57	56	59	58	63	59	55	53	64	64	62	62	64	63
Al	7.8	6.9	5.7	9.6	13	9.8	8.8	12	7.8	4.9	3.5	5.5	5.5	4.9	4.4	4.7	4.2
Si	4.8	0.7	0.9	0.5	0	0	0.7	0.6	1.1	1.7	2.0	10	7.8	5.6	6.7	6.6	6
Ti	0.3	0.3	0.4	0.4	0	0.5	0.4	0	0.5	0.5	1.9	1.9	2.3	1.9	1.9	1.9	1.6
Cr	20	21	21	18	16	16	16	11	16	20	19	6.5	8.1	12	12	10	11
Co	17	18	18	16	15	15	16	13	16	18	17	11	12	14	14	13	14
Y	-	-	-	-	0.7	-	-	0.4	-	-	-	-	-	-	-	-	-
Zr	-	-	-	-	-	-	-	-	-	-	1.1	0.9	-	-	-	-	-
Hf	-	-	-	-	-	-	-	-	-	-	0.2	-	-	-	-	-	-

Note: The column headers span 10–200; the leftmost data column (Ni 50, etc.) aligns under "10".

Table 6
A62 Composition Profile - No Heat Treatment
(in weight percent)

	Nominal Coating	Distance from barrier (in μm)								Nominal Substrate
		21	12	5	3	0	1	6	150	
Fe	70	75	76	77	75	10	-	-	-	-
Cr	18	21	21	18	18	18	26	28	24	24
Al	11	4.6	2.5	5.1	6.3	45	5.0	-	-	-
Co	-	-	-	-	-	24	55	59	60	55
Ni	-	-	-	-	-	-	10	11	11	10

Table 7
A40 Composition Profile - Without Barrier
(in weight percent)

	Nominal Coating	3	19	31	40	56*	79	92	113*	Nominal Substrate
Fe	70	53	52	51	50	50	44	12	0	0
Cr	18	17	17	17	17	16	14	21	24	24
Si	0	1.0	1.0	1.1	1.2	1.0	1.1	3.6	3.8	0
Al	11	4.8	2.8	4.7	5.1	3.8	7.6	2.6	0	0
Co	0	25	24	23	23	25	27	52	61	55
Ni	0	0	4.3	4.1	4.4	4.6	5.8	10	11	10

The column headers 3 through 113* are grouped under "Distance from Surface (in μm)".

Table 8
A19 Composition Profile - with Barrier and Heat Treatment
(in weight percent)

Distance from Barrier (in µm)

		Coating												Substrate				
	Edge	4	20	10	6	4	2	0	1	3	8	12	18	25	30	36	42	58	68
Fe	35	48	49	49	48	47	46	8.0	48	47	30	32	27	26	32	15	0	0	0
Cr	13	17	18	17	17	16	15	3.6	16	16	47	34	50	43	17	19	25	24	25
Si	1.2	1.2	1.1	1.0	1.0	-	1.2	-	1.0	1.2	5.0	3.9	5.8	4.1	2.1	3.3	4.2	4.0	3.7
Al	32	5.8	6.0	6.6	6.0	5.7	7.2	83	8.4	6.3	3.0	4.3	2.2	4.0	3.1	3.2	1.3	0	0
Co	19	25	26	26	25	27	27	5.5	27	26	15	20	15	19	41	53	61	61	63
Ni	0	3.5	0	0	3.5	5.4	3.9	-	0	3.7	0	5.0	0	4.3	5.3	6.3	8.5	12	9.0

Table 9
A19(B) Composition Profile - with Barrier and Heat Treatment
(in weight percent)

Distance from Edge (in μm)

	32	68	96	115	126	130	146	242	Nominal Substrate
Fe	56	55	47	42	38	31	3.6	0.5	0
Cr	18	17	21	9.4	14	27	23	31	24
Si	0.7	1.0	1.5	1.0	1.4	2.7	3.1	3.4	0
Al	4.0	4.2	4.2	7.4	7.3	4.5	1.7	0.2	0
Co	19	20	23	33	33	29	58	55	55
Ni	2.6	2.9	3.5	7.0	7.0	5.9	10	9.8	10

Table 10
Adhesion Strength and Heat Treatments
Cobalt Alloy MAR M509 plus FeCrAlY

Sample	°C	Hrs	Atmosphere	Thermal Oxide μm	Sputtered Oxide μm	Adhesion Oxide MPa	Adhesion Pt MPa
A4	1075	40	air	0.9	-	70	1.8
A15	1050	66	Ar	0.9	2.8	60	65.0
A19	1050	66	Ar	0.9	-	-	-
A28	1070	50	air	1.1	-	-	-
A35	1070	60	Ar, air	1.5	-	-	-
A38	1120	25	Ar, air	heavy, mixed	-	-	-
A40	1065	47	air	1.8	2.3	-	-
A42A	1050	80	Ar+H_2O	1.6	-	-	-
A43	1065	46	Ar	<1	2.0	62	-
A43A	1090	50	Ar	1.9	2.6	39	17.8
A52	1090	66	Ar+H_2	1.0	dark	-	-
A63	1025	48	air	(3)*	dark	-	-

*heavy oxide on uncoated edge

Table 11
Adhesion Strength and Heat Treatments
Nickel Alloy MAR M200+Hf plus FeCrAlY

Sample	°C	Hrs	Atmosphere	Thermal Oxide µm	Sputtered Oxide µm	Adhesion Oxide MPa	Adhesion Pt MPa
B10	1090	66	air	1.6	-	-	-
B14	1060	50	air	3.0	-	-	-
B16	1060	47	air	2.0	0.8	>70	32
B23	1077	50	air	-	-	-	-
B27	1025	48	air	1.2	-	-	-
B27A	1090	50	Ar+H$_2$O	1.0	2.5	>70	-
B36	1050	80	Ar+H$_2$O	-	-	-	-
B38	1065	46	Ar	0.4	<1	-	-
B41	1070	62	Ar, air	2.0	-	-	-
B43	1120	25	air	-	-	-	-
B45	1075	50	air	2.5	3.0	67	-
B47	1050	66	Ar+H$_2$O	2.0	1.1	68	62
B49	1075	40	air	2.0	rough	66	low

Table 12
Adhesion Strength and Heat Treatments
Nickel Alloy MAR M200+Hf plus NiCoCrAlY (EB)

Sample	°C	Hrs	Atmosphere	Thermal Oxide μm	Sputtered Oxide μm	Adhesion Oxide MPa	Adhesion Pt MPa
C11	1120	25	Ar,air	Green, Defective	-	-	-
C12	1090	25	Ar+H$_2$O	1.1	2.8	64	45
C13	1075	50	air	2.8	2.6	>70	-
C14	1075	50	air	2.7	2.8	69	-
C15	1075	40	Ar,air		5.5	66	low
C18	1025	48	air	3.3	-	-	-
C19	1025	48	air	2.1	1.9	>70	55
C20	1125	63	air	-	0.6	69	>70
C21	1075	49	Ar,air	2.2	-	-	-
C22	1065	46	Ar	0.1	1	3.6	3.4
C23	1075	49	Ar,air	2.0	1.5	>70	-
C24	1065	47	air	2.4	0.8	55	25.5
C25	1090	66	Ar+H$_2$	1.3	Damaged	-	-
C26	1050	80	Ar+H$_2$O	1.0	1.2	-	-
C28	1050	66	Ar	0.4	3.0	35	-

Table 13
Adhesion Strength and Heat Treatments
Nickel Alloy MAR M200+Hf plus NiCoCrAlY (S)

Sample	°C	Hrs	Atmosphere	Thermal Oxide μm	Sputtered Oxide μm	Adhesion Oxide MPa	Adhesion Pt MPa
D1	1050	80	Ar+H_2O	2.6	-	-	-
D2	1025	50	air	2.7	1.9	15.6	-
D3	1025	50	air	2.0	-	67.0	-
D4	1090	50	Ar+H_2O	3.2	1.5	-	-
D5	1125	63	air	3.5	-	62.0	65
D6	1075	50	air	2.9	-	-	-
D7	1075	49	Ar,air	3.6*	-	-	-
D8	1075	49	Ar,air	2.9*	-	-	-

* Blue contamination
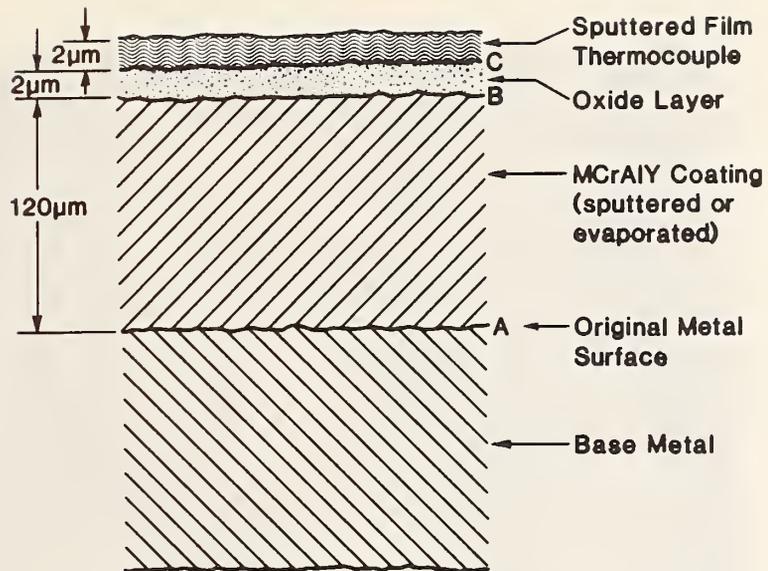
Figure 1. Schematic cross section of thin film sensor

Figure 2. NiCoCrAlY coating on Ni alloy
Nickel backing is on top. Test sample heat treated 4 hours in argon (500x)
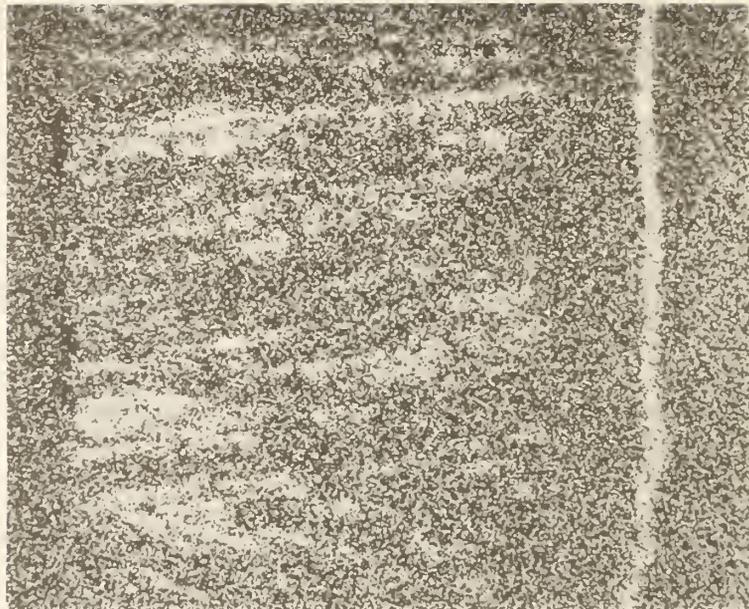
Figure 3. Yttrium X-ray Map of NiCoCrAlY coating
as deposited with Ni backing (860x)

Figure 4. Sputtered FeCrAlY coating on Ni alloy
Ni backing on top. Notice faceted growth (1000x)
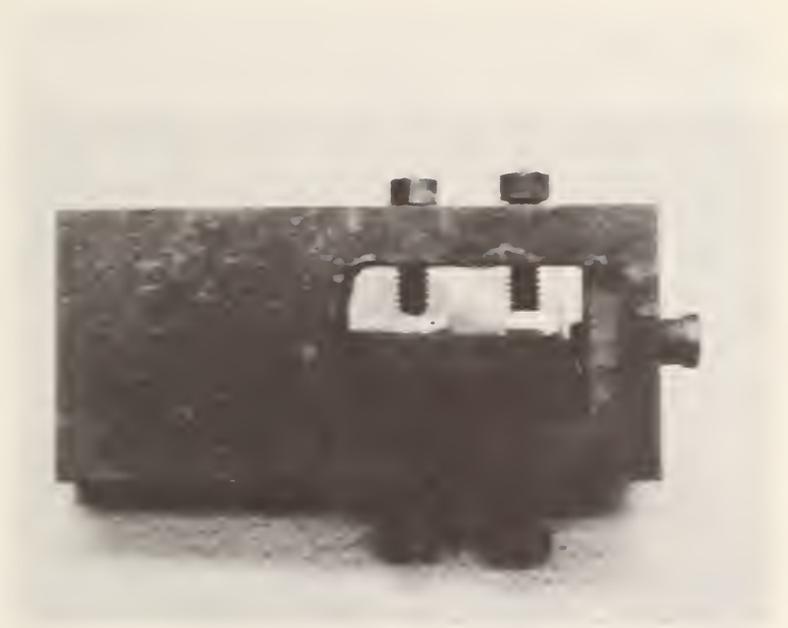
Figure 5. High temperature electrical test fixture

Figure 6. Electron scan of D24 (1100x)
Al highlighted displaying Al₂O₃ phase

Figure 7. Scanning electron micrograph of D4 (1530x)
Oxides are penetrating inward from surface
Heat treated at 1090°C for 50 hours

Figure 8. Al Map of D4 (1530x)
Al_2O_3 penetration evident from diffusion pipes
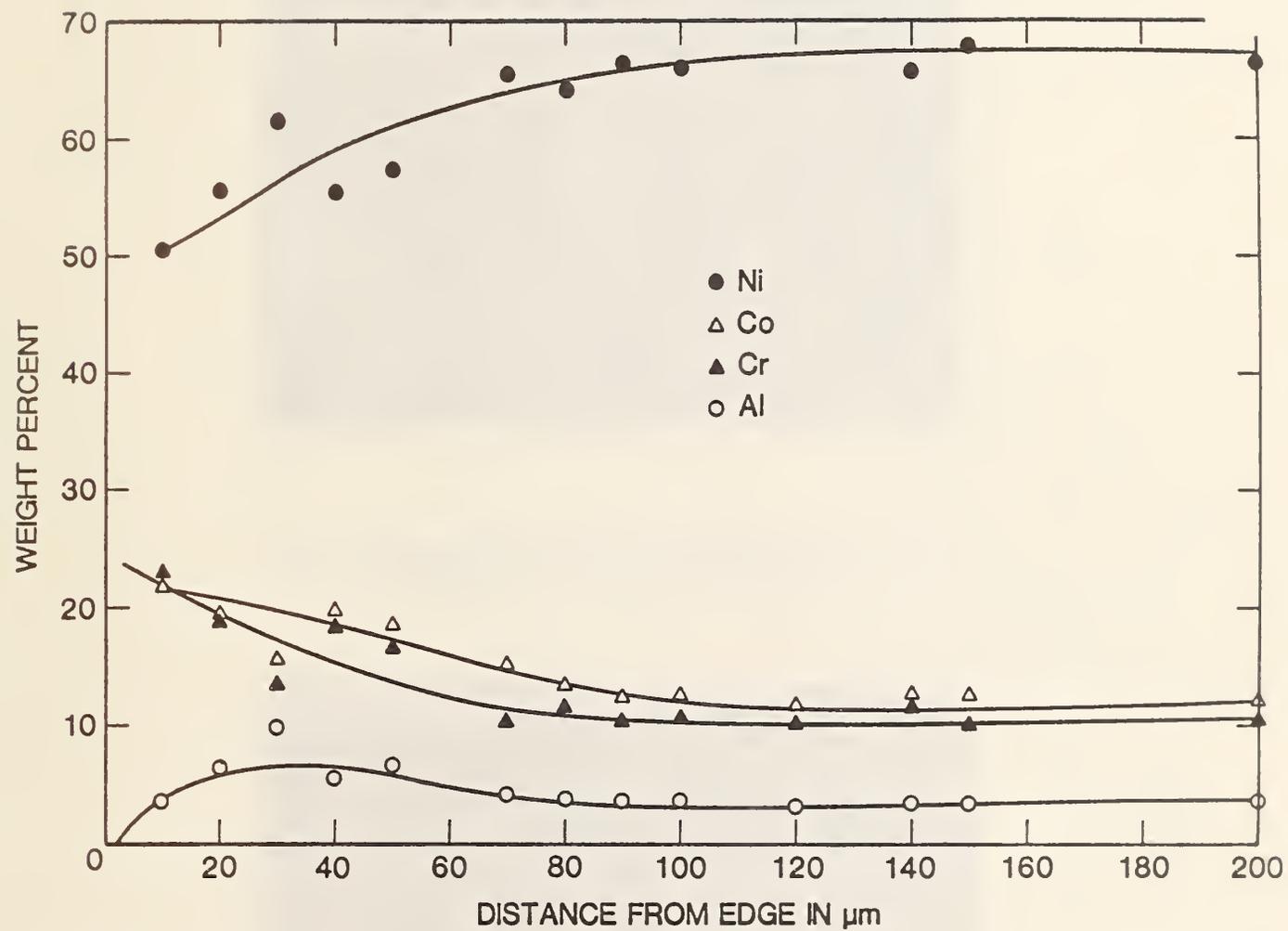
Figure 9. Diffusion profiles of D4
Heat treated at 1090 for 50 hrs without barrier

Figure 10.   Scanning electron photograph of D14
Al_2O_3 is dark 1 μm line 580x

Figure 11.   Al map of D14 (580x)

Figure 12. Co map of D14 (580x)

Figure 13. Cr map of D14 (580x)
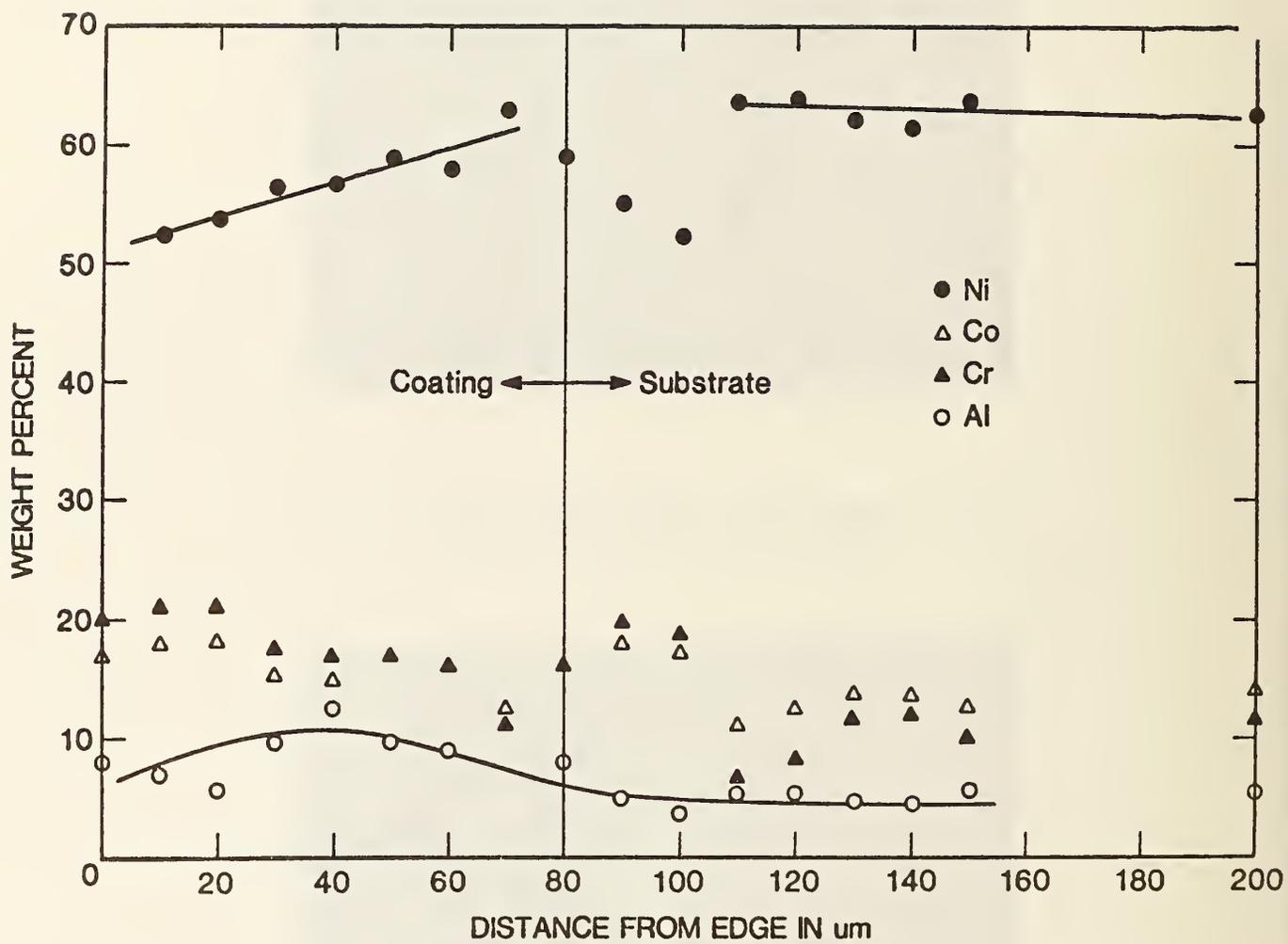
Figure 14. Diffusion profiles of D14.
1 μm barrier layer 1080°C, 50 hrs
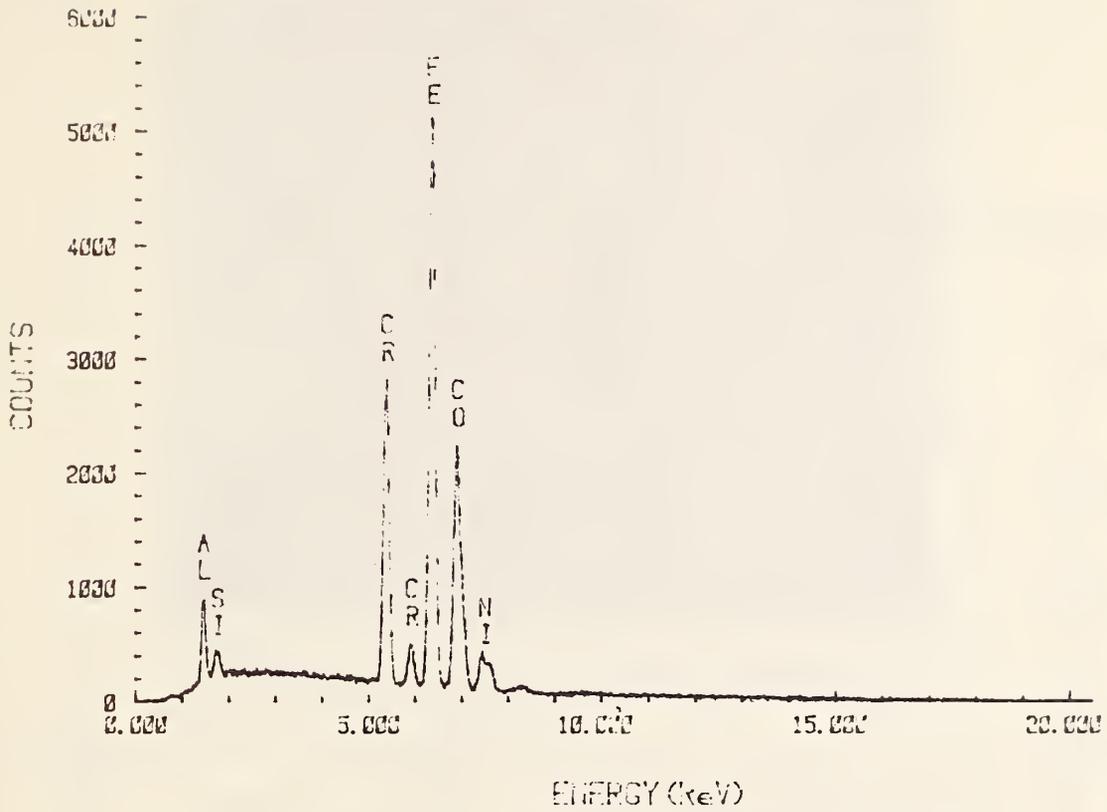
Figure 15. EDX intensity vs. energy of A40 in coating
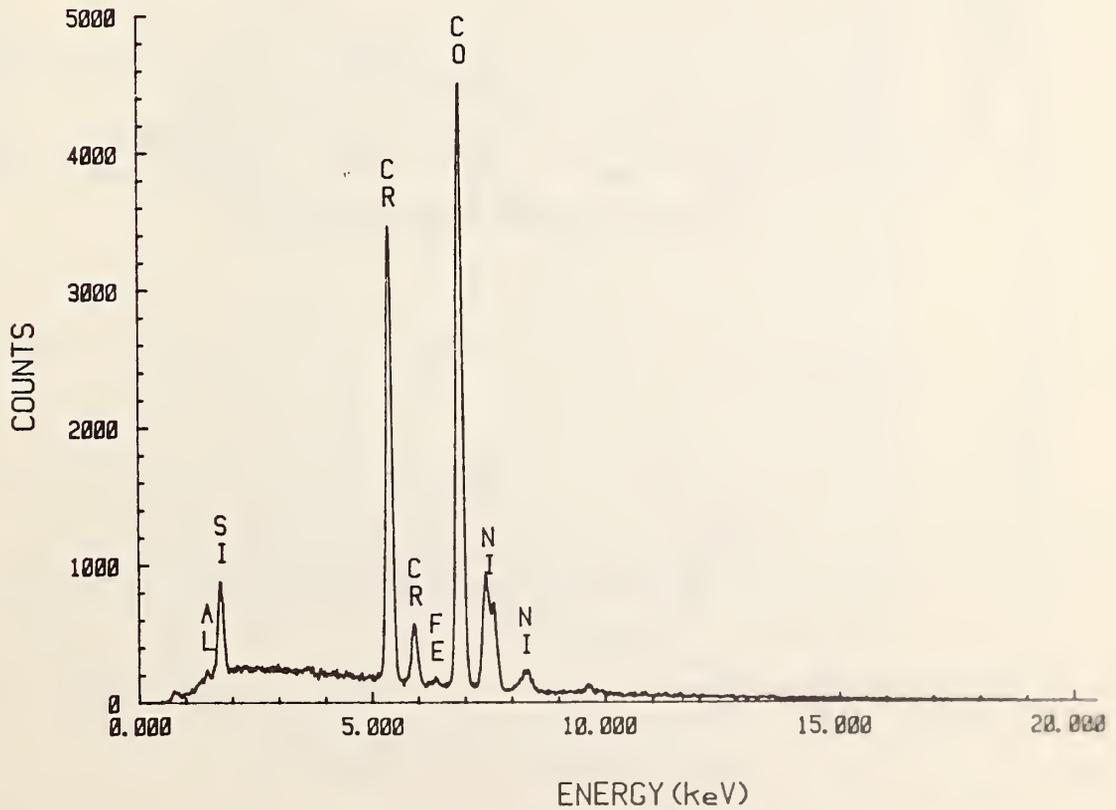
Figure 16. EDX intensity vs. energy of A40 in substrate material
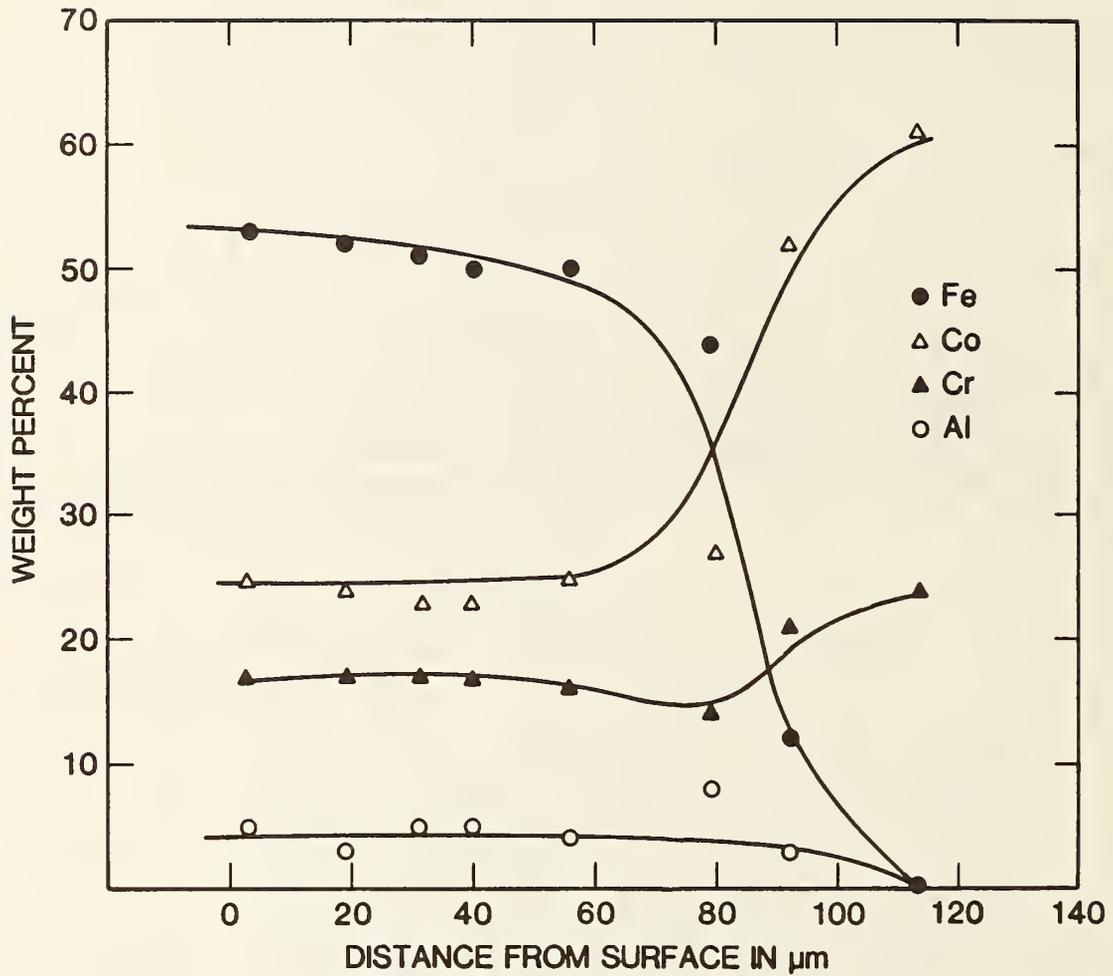
Figure 17. Diffusion profiles of A40
No barrier layer, 1075°C, 50 hrs

Figure 18. Scanning Electron Micrograph of A19
Note bridging of Al_2O_3 barrier layer with metal
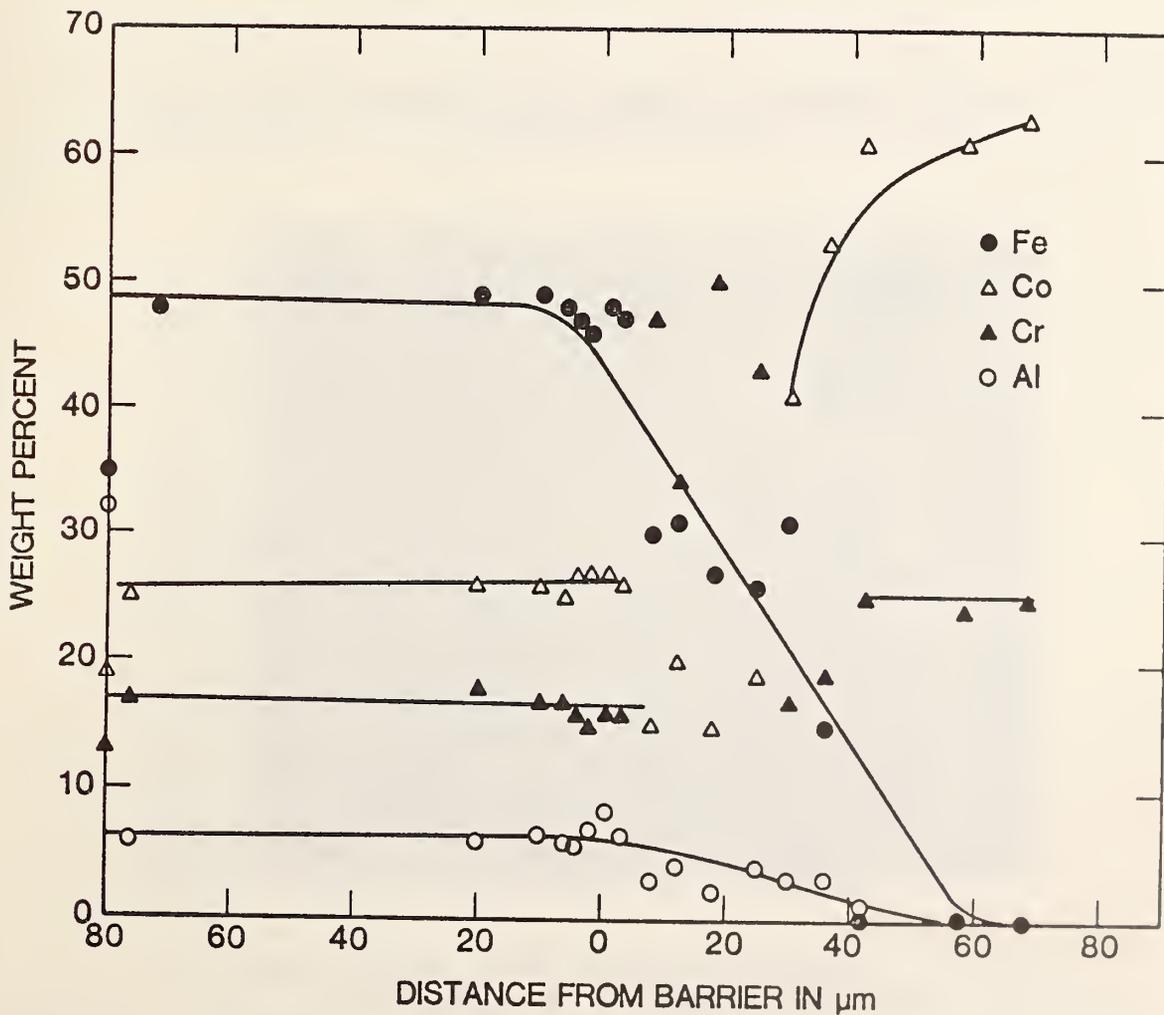
Figure 19. Diffusion profiles of A19
2 μm barrier, 1075°C, 86 hrs
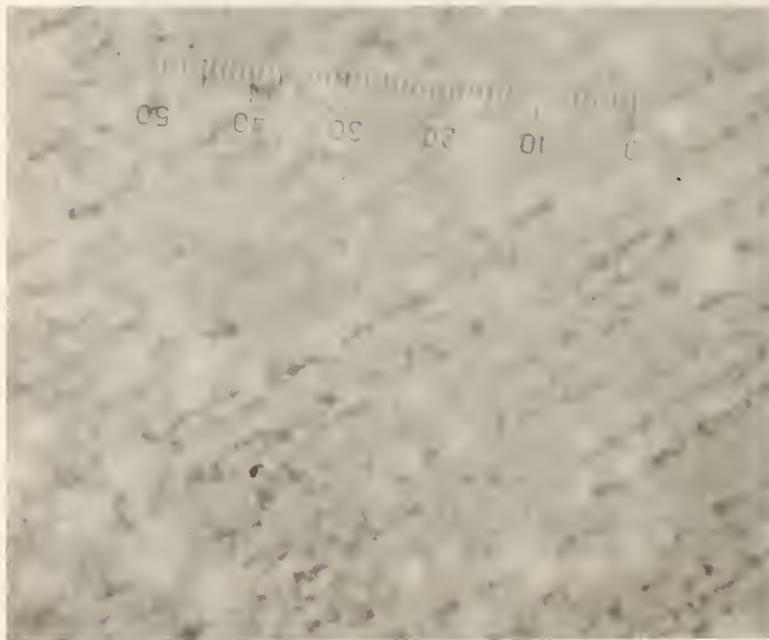
Figure 20.   Thermal oxide on A4 uneven oxide due to surface grooves from polishing (500x)
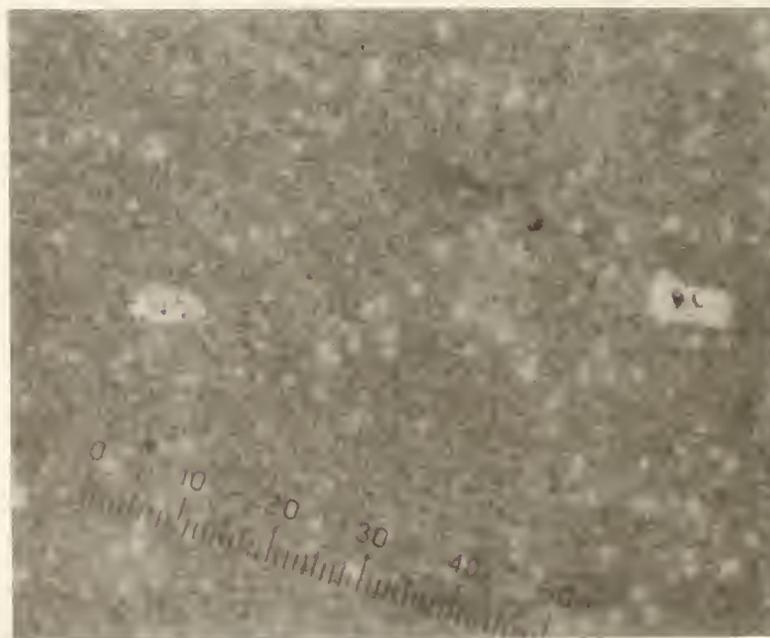
Figure 21.   Thermal oxide spalling of FeCrAlY sample A35
Note holes under spalled areas (100x)

Figure 22.   Thermal oxide of FeCrAlY on FeCrAlY on B10
Dark grains are related to uneven growth pattern (500x)

Figure 23.   Thermal oxide of FeCrAlY on B41 oxide is 2.0 μm Thick (250x)

Figure 24. Thermal oxide of electron beam deposited NiCoCrAlY on C21
Small fibrous habit of oxide apparent in addition to film growth (500x)

Figure 25. Thermal oxide of sputtered NiCoCrAlY on D8
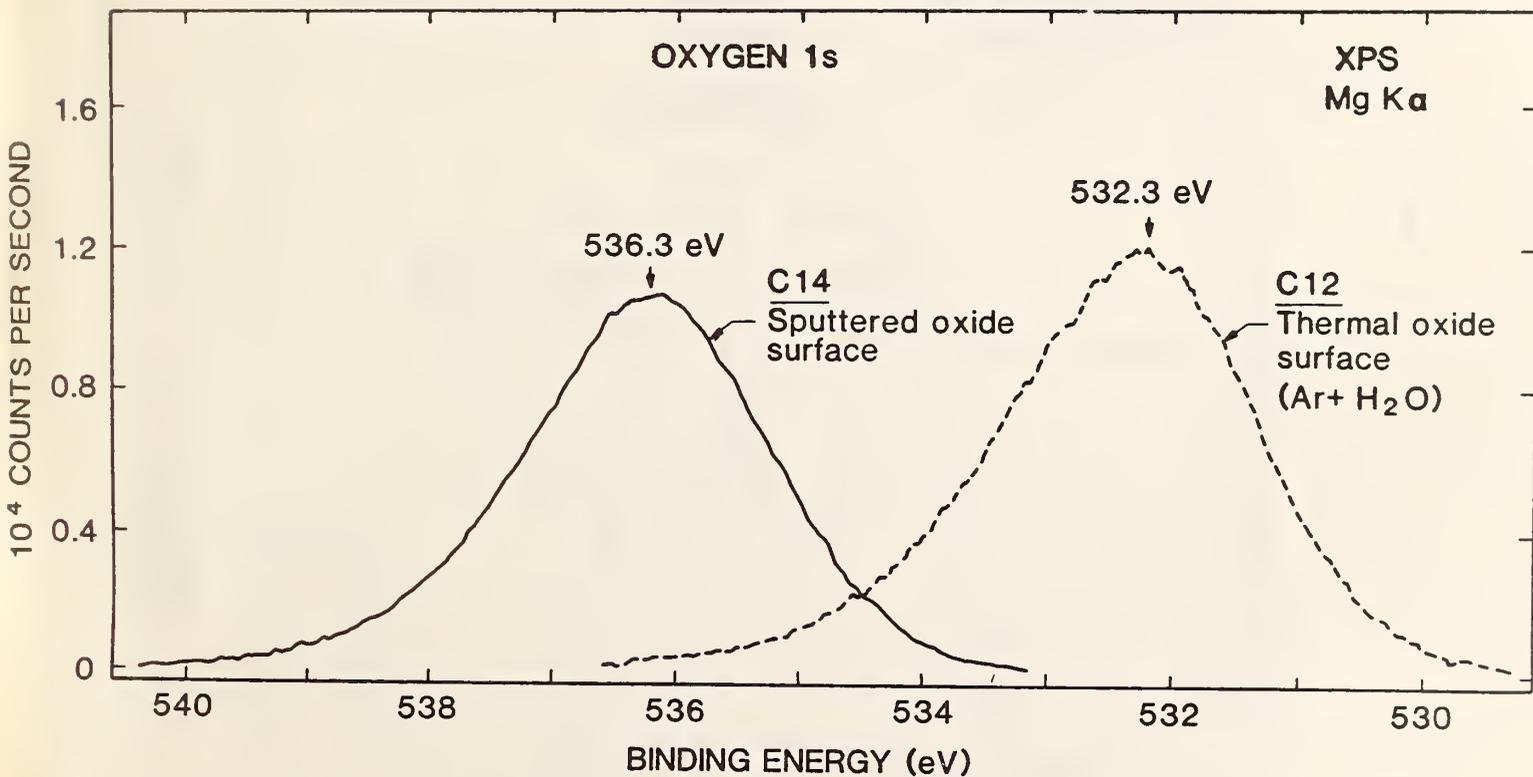
Figure 26. Oxygen 1s XPS core levels from samples C12 and C14. The better insulating properties of the C14 sputtered oxide surface lead to an upward shift in binding energy which positions the O1s level 4 eV higher than O1s level from the Ar+H_2O thermal oxide at the surface of C12. Similar shifts were observed in comparisons of other features (e.g., C1s) derived from these samples.
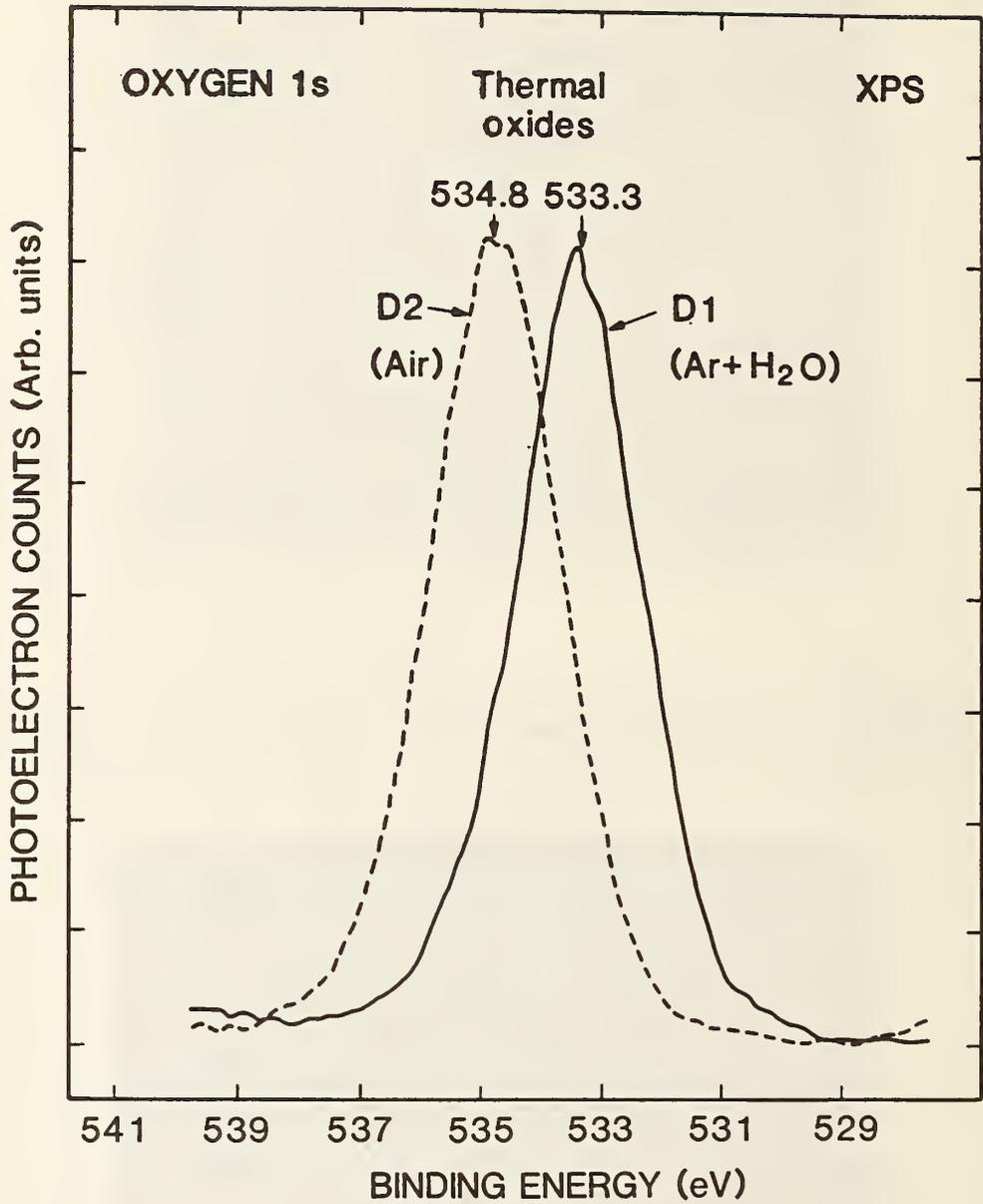
Figure 27. Comparison of the O1s levels for samples D1 and D2. The D2 oxide grown in air has a larger charging shift than the D1 oxide grown in Ar and H₂O. Similar shifts occur between the C1s and other core levels for these samples.
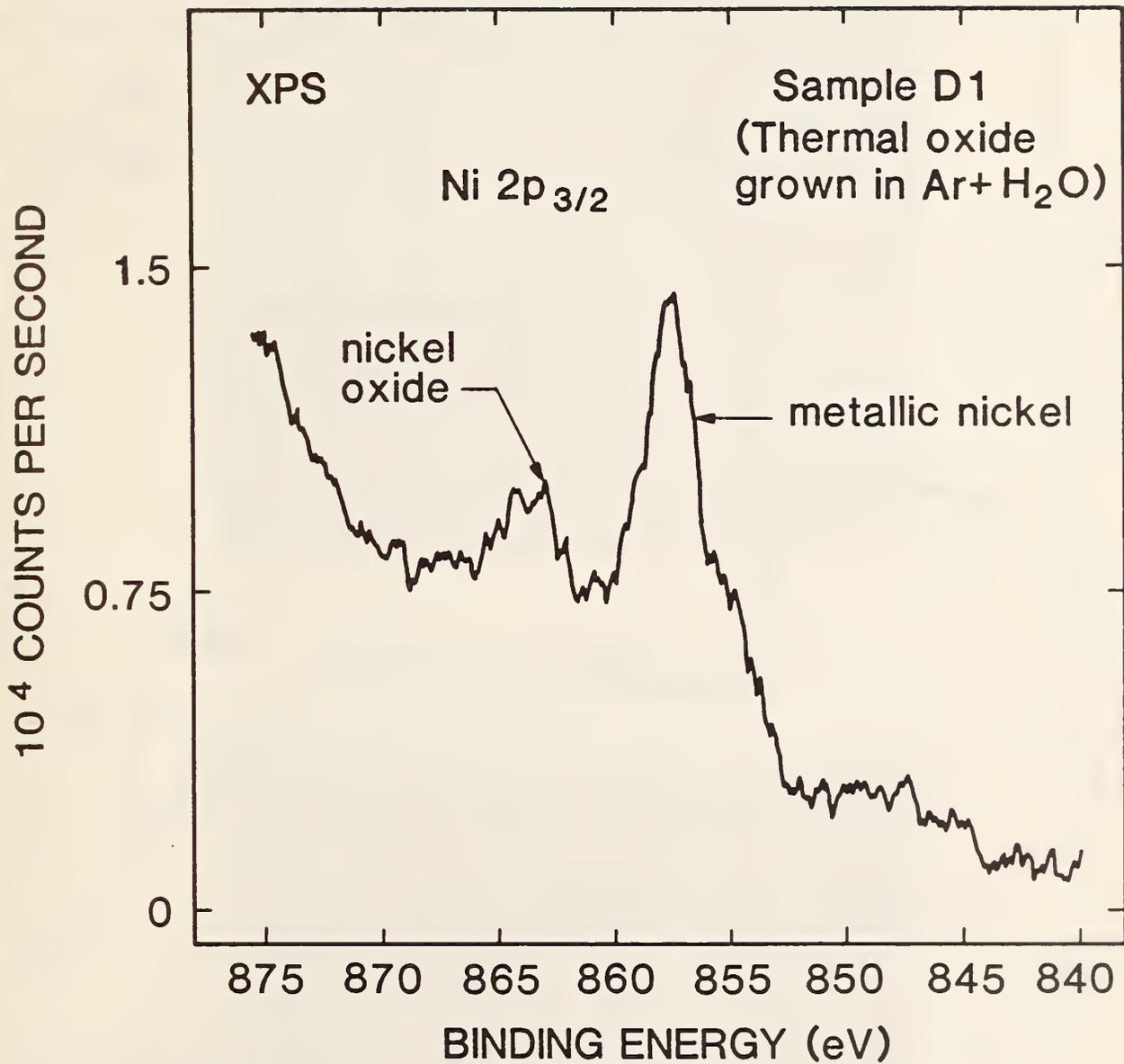
Figure 28. XPS nickel 2p3/2 core level region indicating the presence of metallic and oxidized nickel in the surface aluminum oxide of sample D1.
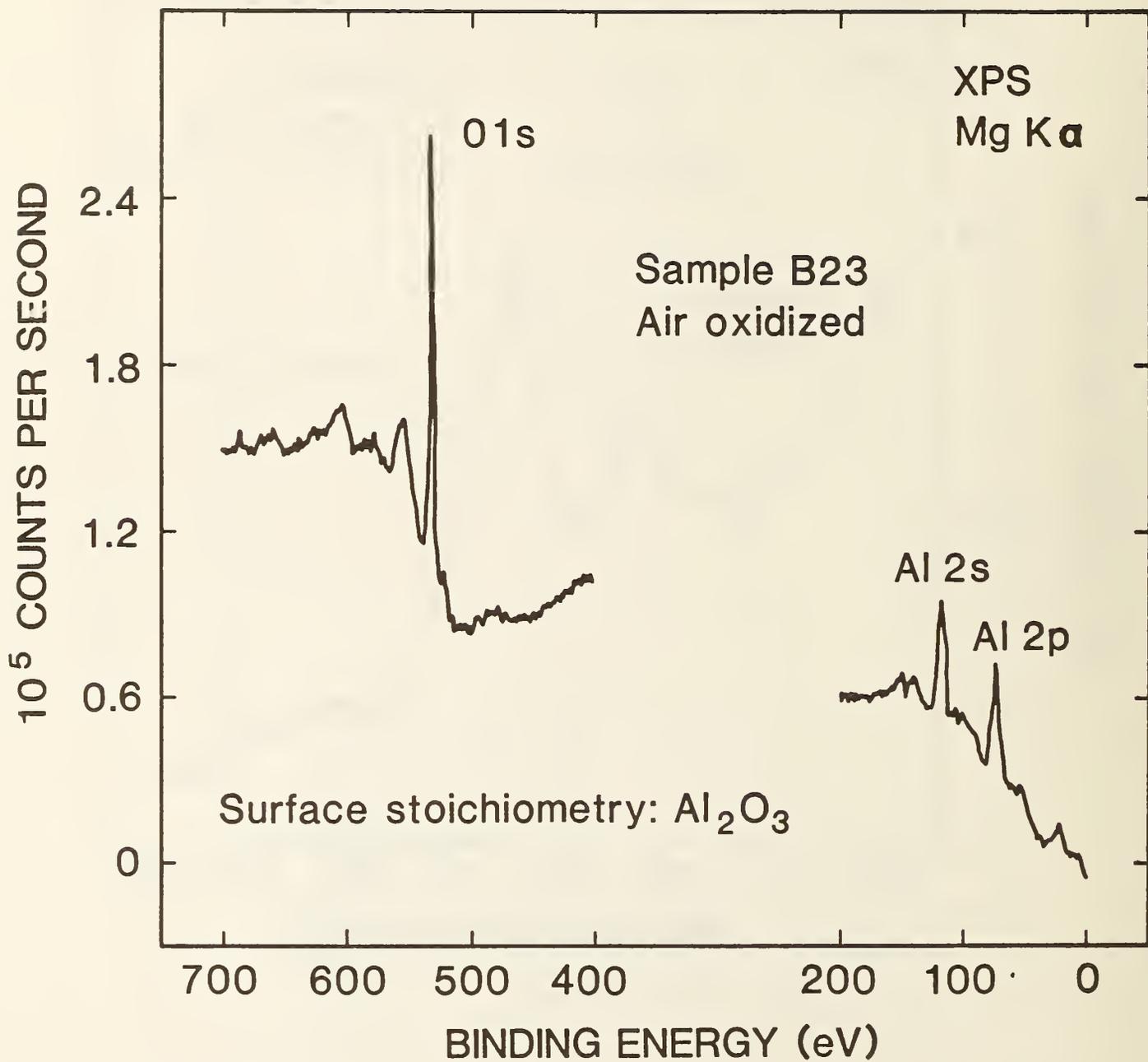
Figure 29. Wide energy range XPS spectrum obtained from the air-oxidized
surface of sample B23. The 01s and Al features indicate
an Al₂0₃ stoichiometry at the surface.

Figure 30. Sputtered oxide on A43A
Note smooth pebbly film (500x)

Figure 31. Sputtered oxide on C19
Similar to A43A (500x)
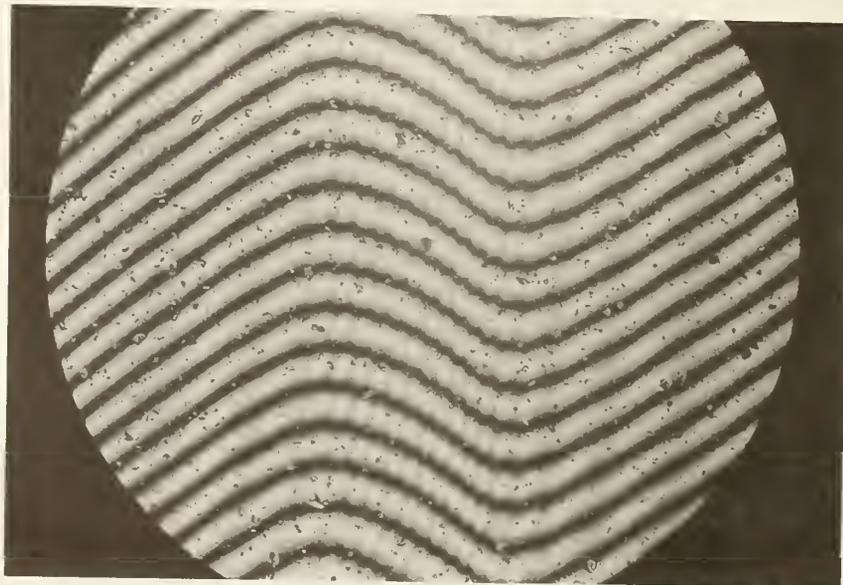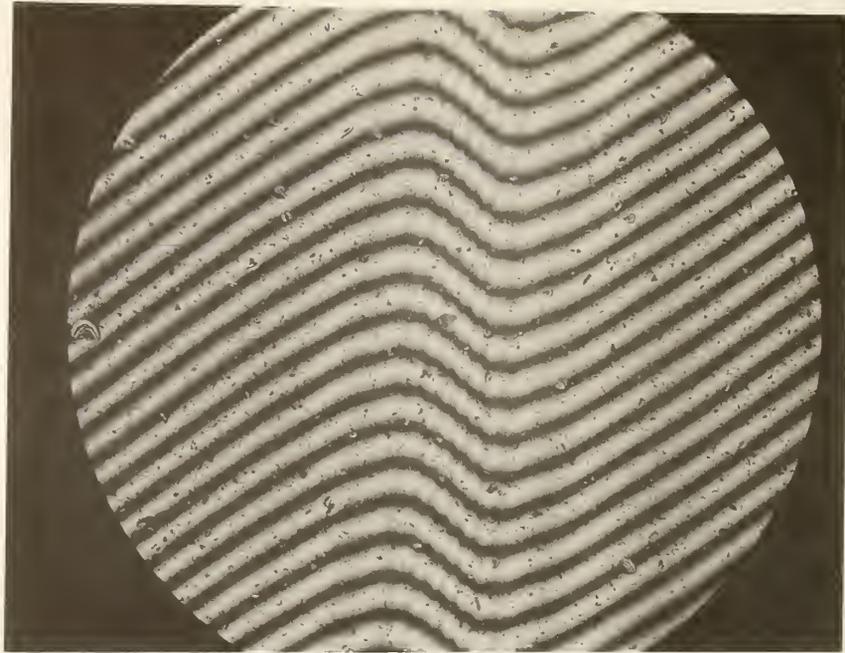
Figure 32. Interferometric micrographs of sputtered aluminum oxide.
Above indicates 1.6 μm thick; below indicates 1.9 μm thick
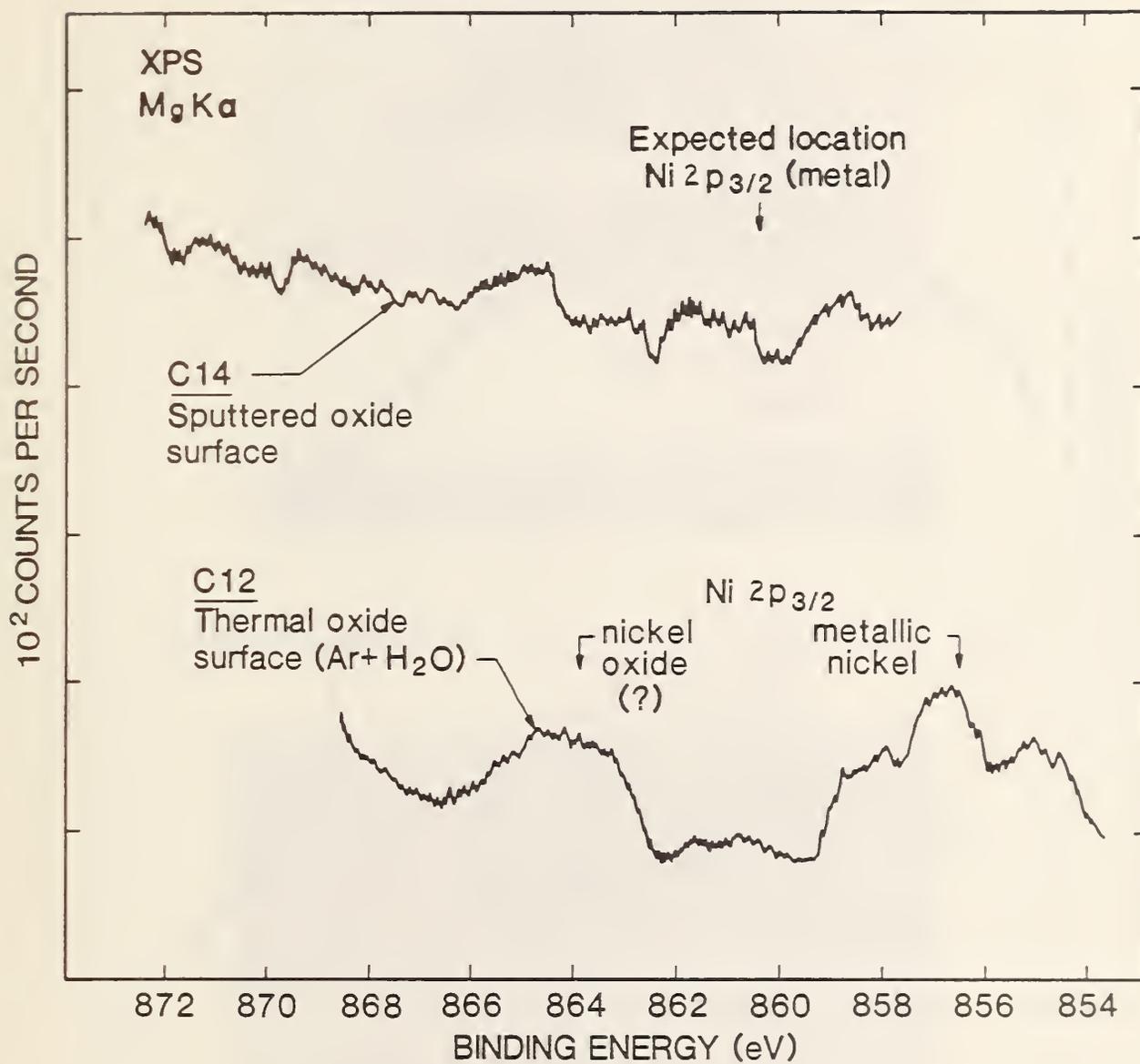
Figure 33. XPS spectra for samples C12 and C14 in the binding energy region near the Ni2p3/2 level. The thermally oxidized C12 surface has Ni present at an estimated level near 0.5%, while essentially no Ni is observed in the sputtered aluminum oxide on C14.
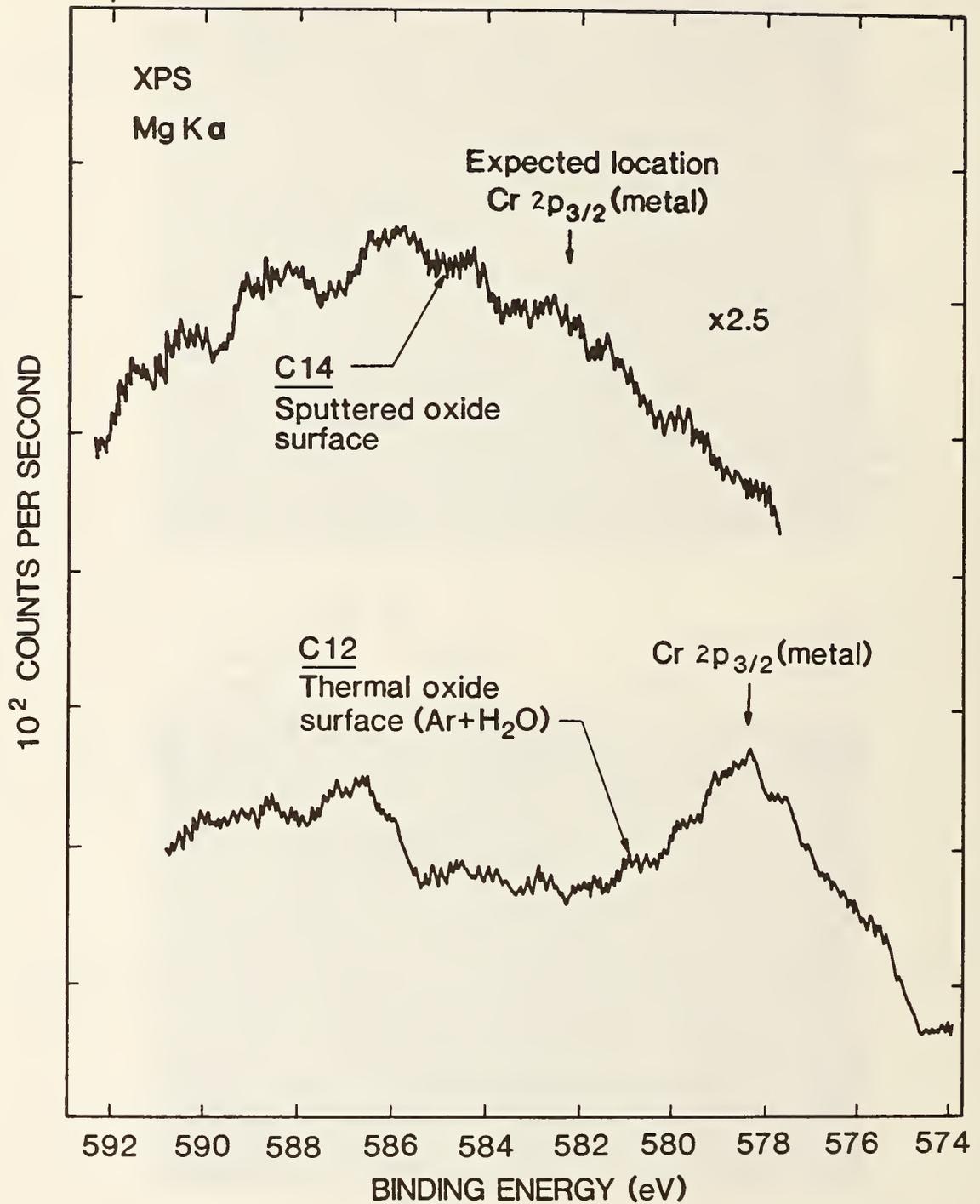
Figure 34. XPS spectra for samples C12 and C14 in the binding energy region near the Cr2p$_{3/2}$ level. The feature in the C12 spectrum indicates a Cr concentration in the thermal oxide near 0.5%, while Cr appears to be completely absent from the sputtered oxide surface of C14.

Figure 35. Small test coupon for thin film Pt and Pt 10% Rh

Figure 36. Thin film thermocouple test coupon

Figure 37. Sputtered oxide film resistance

4. TITLE AND SUBTITLE

Advanced Thin Film Thermocouples

5. AUTHOR(S)

Kenneth G. Kreider, Stephen Semancik, and Craig Olson

11. ABSTRACT *(A 200-word or less factual summary of most significant information. If document includes a significant bibliography or literature survey, mention it here)*

Abstract

The fabrication, materials characterization, and performance of thin film platinum-platinum rhodium thermocouples on gas turbine engine alloys has been investigated. The materials chosen for the study were the turbine blade alloy systems MAR M200+Hf with NiCoCrAlY and FeCrAlY coatings; and vane alloy systems MAR M509 with FeCrAlY. Research was focussed on making improvements in the problem areas of coating-substrate stability, adhesion, and insulation reliability and durability. Diffusion profiles between the substrate and coating with and without barrier coatings of Al_2O_3 are reported. The relationships between fabrication parameters of thermal oxidation and sputtering of the insulator and its characterization and performance are described. The best thin film thermocouples were fabricated with the NiCoCrAlY coatings which were thermally oxidized and sputter coated with Al_2O_3.

12. KEY WORDS *(Six to twelve entries; alphabetical order; capitalize only proper names; and separate key words by semicolons)*

high temperature sensors; reactive sputtering; thermocouples; thin film thermocouples; turbine alloy coatings; turbine engine sensors